1987

Non-destructive evaluation of notched aluminum specimen by application of electromagnetic discharge imaging /

Chun-Hung Kuo
Lehigh University

NON-DESTRUCTIVE EVALUATION OF NOTCHED ALUMINUM SPECIMEN BY APPLICATION OF ELECTROMAGNETIC DISCHARGE IMAGING

by

Chun-Hung Kuo

A Thesis

Presented to the Graduate Committee

of Lehigh University

in Candidacy for the Degree of

Master of Science

in

Department of Mechanical Engineering and Mechanics

Lehigh University

1987

This thesis is accepted and approved in partial fulfillment of the requirement for the degree of Master of Science.

July 2, 1987
(date)

George C. Sih
Professor in Charge

F. Erdogan
Chairman of Department

ACKNOWLEDGEMENTS

The author wishes to thank his advisor, Professor George C. Sih, for his encouragement, guidance and discipline throughout the course of this investigation.

The advice and assistance of Dr. John Michopoulos has also been most appreciated.

The author is especially thankful to Dr. Ya-Yen Lee of M. D. Anderson Hospital at Texas Medical Center. Without his most careful treatment, the author would have not made his return to Lehigh possible. The large number of people who have been caring for him in the past three years makes it impossible to mention each by name.

The author is particularly grateful to his family in Taiwan for their support in the period of his graduate program at Lehigh.

The secretarial assistance from Mrs. Barbara DeLazaro and Connie Weaver is greatly appreciated.

TABLE OF CONTENTS

LIST OF TABLES

LIST OF FIGURES

LIST OF FIGURES - (CONTINUED)

ABSTRACT

The Electromagnetic Discharge Image (EDI) is applied for the non-destructive detection of precut notches in 6061 aluminum plate specimens. This involves the application of a high frequency and high voltage A.C. signal to the specimen whereby the electrical discharge can be recorded photographically. The results reflecting the topography and dielectric structure of the notched specimen is then processed such that their physical implications in terms of changes in the thermal/mechanical/electrical/effects can be interpreted.

Obtained theoretically is the electric field intensity distribution of the notched aluminum specimen by numerically solving a nonlinear differential equation governing the electrical potential. The change in the depth of the notch is reflected by the spatial distribution of the electric field. Comparisons are made with the light intensity distribution determined experimentally by EDI. Various parameters affecting the emitted image are investigated in addition to change in the excitations of the wave form. Determined is the combination of these parameters that yield the optimum results from the viewpoint of pattern recognition as compared with the theoretical prediction. Change in notch depth is clearly recognizable from the discharge image pattern. A direct correlation can be established between the notch depth and change in the local amplitude of the electric field and the light field intensity. Three-dimensional effects that are not so easily assessed by analytical means can be more readily detected by the EDI method.

CHAPTER I - INTRODUCTION

The process of Electromagnetic Discharge Image (EDI) is concerned with the application of a high-voltage electrical field such that electrons in the neighborhood of the subject or object under investigation are accelerated and multiplied exponentially creating an avalanche. Streamers are created and the phenomenon can be recorded photographically or digitally. It was also known in its early days of development as Kirlian photography which was mostly associated with the study of biological subjects. A detailed historical account of the EDI method and its related theoretical considerations can be found in two technical reports [1,2] published by the Institute of Fracture and Solid Mechanics (IFSM), Lehigh University.

The research on EDI at the IFSM was initiated in the early 1980's from a DOD grant that provided the seed money for the equipment. One of the main objectives of this effort was to use EDI as a nondestructive evaluation (NDE) technique. The early works in both the U.S.S.R. [3,4] and U.S.A. [5,6] lacked the theoretical support without which the technique remains as empirical. Well-controlled experiments are needed such that the sensitivity of the dielectric air gap between the specimen and the electrodes, applied voltage and frequency can be assessed quantitatively in terms of the resulting image. Of particular interest is the detection of the shape, size and location of defects such as cracks, microvoids and other types of imperfections in the material. The ultimate goal is to provide a record of the mechanical inhomogeneity which can be incorporated into the appropriate computer software

for an evaluation of the mechanical integrity of structural components or systems. Initial success [7] has already been achieved in detecting imperfections that were introduced mechanically by drilling holes of different sizes and chemically by applying corrosive agents to aluminum specimens.

The work to be reported in this thesis is concerned with the EDI detection of notch configuration and size in aluminum specimens. The pulse duration, peak-to-peak voltage, frequency and air gap are varied so that the resolution and quality of the resulting image can be optimized. Theory and experiment are then compared. The initial agreement is encouraging and suggests the possibility of applying the EDI technique for analyzing defects and material inhomogeneities in three dimensions.

CHAPTER II - ELECTROMAGNETIC DISCHARGE IMAGE

The method of EDI involves the collision of electron ions and photons or gas molecules. Such a process is highly sensitive to the air gap distance between the electrode and specimen which affects the forces or kinetic energy generated from the electric and magnetic field. Parameters associated with the wave form and specimen properties will also have a direct influence on the discharge image.

2.1 Influence of Specimen

Only the major variables that affect the EDI process will be discussed.

Dielectric Property. The dielectric property of the specimen determines conductive nature of the material. When an alternating electric field is applied, the dipoles and free charges in a medium are excited, depending on the frequency. Both electric resistance and dielectric hysteresis will necessarily be present [8-10]. The former is known as conduction loss (CL) and the latter as dielectric loss (DL). A medium is regarded as a conductor if CL > DL, a semiconductor if CL ≃ DL, and a dielectric if CL < DL.

As mechanical defects or imperfections affect the dielectric properties of the material, material inhomogeneities can be reflected by the EDI.

Mechanical Inhomogeneities. Since the specimen surface itself may act as one of the electrodes, any surface irregularities such as voids

and roughness may alter the air gap or the transmission of the electrons. Electrostatic carriers also tend to concentrate on sharp edges, cracks or any other locations that involve sudden change in curvature. This gives rise to a local intensification of photons in the ionization process. Variations in light intensity will thus depend on abrupt changes in the physical geometry of the specimen.

Inhomogeneity arising from the material microstructure will also affect the rate of ionization and change the local dielectric and diamagnetic distribution. The scale level at which this alteration occurs is proportional to the physical dimensions of the material inhomogeneity and its distribution.

2.2 EDI Instrumentation

A circuit diagram of the EDI instrumentation is shown in Figure 1. It consists of a function generator, pulse generator, power amplifier and oudin coil. The voltage difference of the power amplifier can vary from 200 volts R.M.S. to 20-25 K volts R.M.S. The power amplifier is driven by the function generator and pulse generator such that any possible pattern of wave form, from single pulses and continuous wave forms to bursted or gated unipolar or bipolar frequency sweep and varying amplitude wave packets can be obtained.

Waveform Pattern. The potential applied to the electrodes can generate various different characteristics of the wave form. They can be sinusoidal, triangle, rectangular or even arbitrary in shape. Different wave packets can be formed with different time of duration.

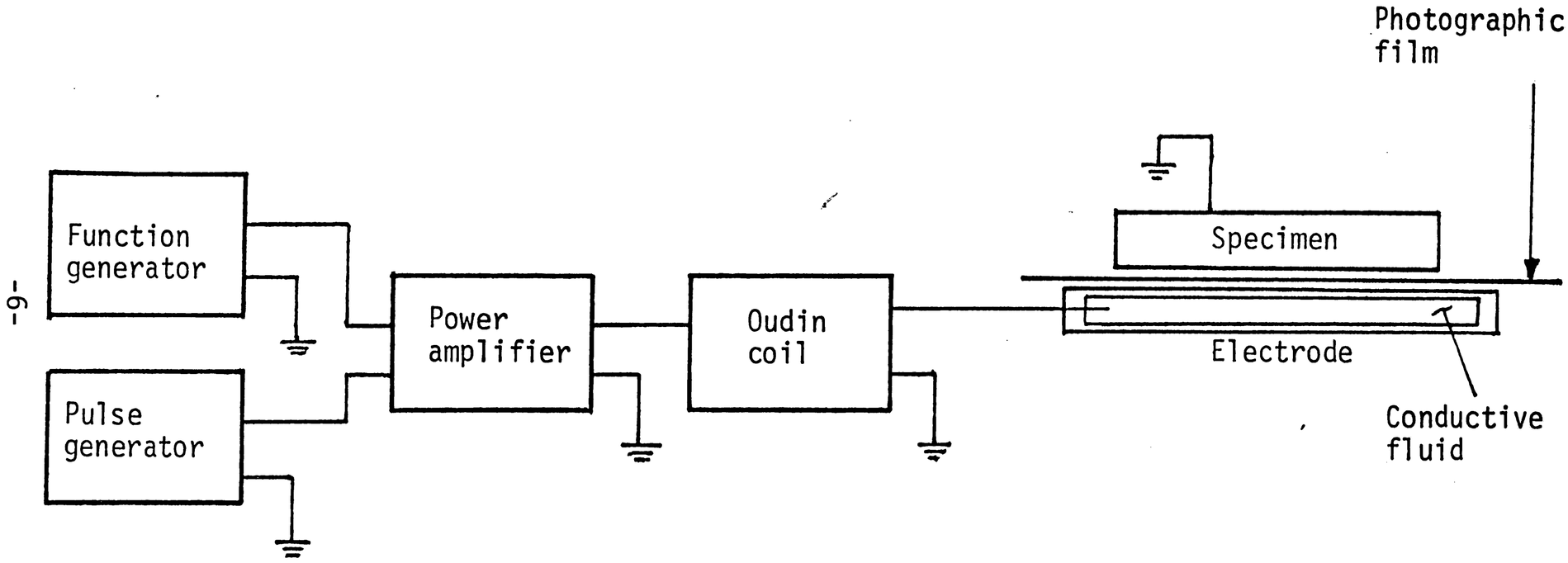

Figure 1 - Instrumentation setup.

Several characteristics of the wave form can be generated. Shown in Figure 2 is a typical example. The first wave packet contains the largest amplitude in the first of the three cycles while the second packet has six cycles with decreasing amplitudes. The last wave packet includes approximately eight cycles with decreasing amplitude. They are labelled, respectively, as I, II and III in Figure 2. The time interval between identical wave packets is the pulse rate. It can vary from 5 μsec to 10 msec depending on the frequencies of the wave packets. The different excitations will be discussed subsequently.

Direct Contact. The direct contact method* [1] will be used such that the lower electrode consists of two 1 mm thick glass plates with a transparent conductive fluid sandwiched in between as shown in Figure 1. A saline water solution is used. This electrode is then connected to the wave form generator. The upper electrode is the specimen that is grounded. A photographic film is inserted between the electrode and specimen with the photographic emulsion facing the specimen. Under these conditions, the corona discharge from the specimen as shown in Figure 2 is exposed directly to the photographic emulsion. An ASA 125 Kodak Plus-X negative film can be used.

*Other methods of EDI can be found in [11-14].

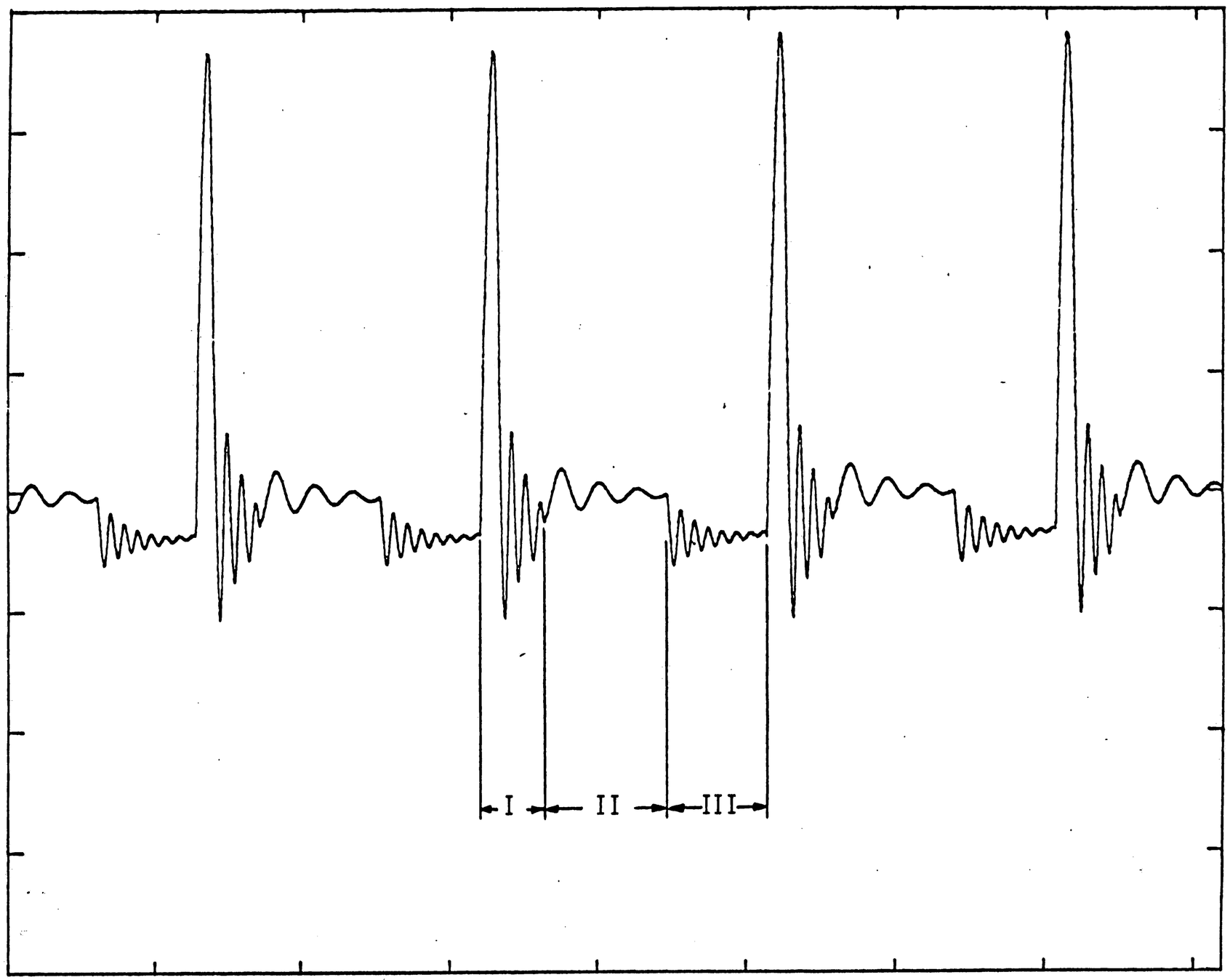

Figure 2 - Typical wave form of applied electric field.

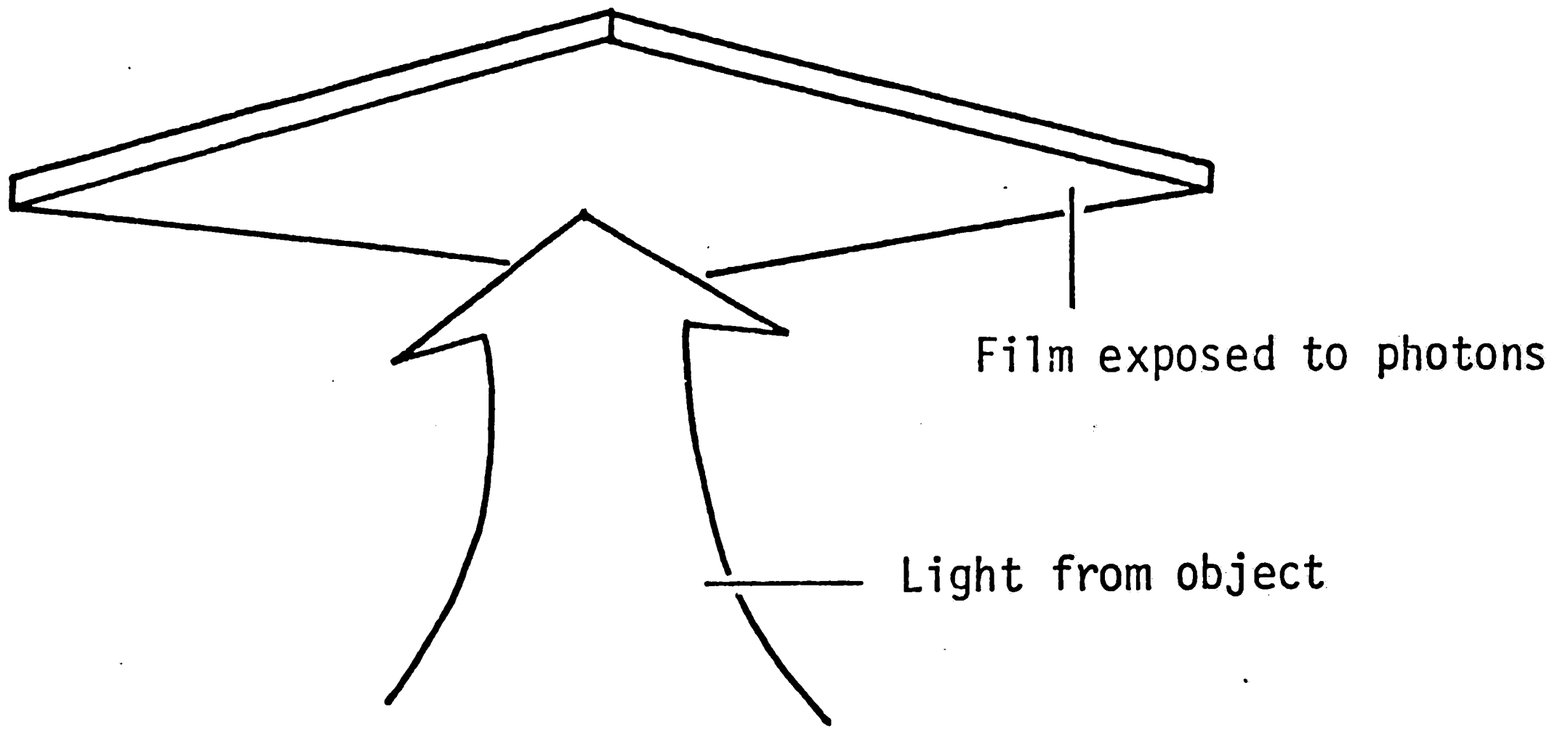

Figure 3 - Image created by emission of photons from specimen.

CHAPTER III - STATEMENT OF PROBLEM

To be analyzed by the EDI method are the characteristics of pre-cut notch in plate specimens made of 6061 aluminum alloy. The electric potential field is first obtained analytically by solving a differential equation of the Poisson type, the solution of which is then compared with the experimental results. Electric and light intensity are altered to show their effects on the discharge image.

3.1 Notch Geometry

More specifically, two different notch type 1 and 2 are considered. The dimensions a and b of the notch and of the specimen are given in Figure 4. Figure 5 shows the notch position with reference to the film and electrode while an enlarged view of the set-up is given in Figure 6.

3.2 Excitation Settings

Four different excitation settings of the wave form in Figure 2 are used. Their characteristics are displayed in Figure 7 and referred to as A, B, C and D. The numerical values of the pulse duration and peak-to-peak voltage of each wave packet can be found in Table 1.

3.3 Objective

The objective of this investigation is outlined by the flow chart in Figure 8. Results pertaining to the discharge image of the notched specimen in Figures 4 to 6 will be obtained theoretically and experi-

Notch Type	Notch Size	
	Width (2a)	Depth (b)
1	1.5 mm	1.50 mm
2	1.5 mm	.75 mm

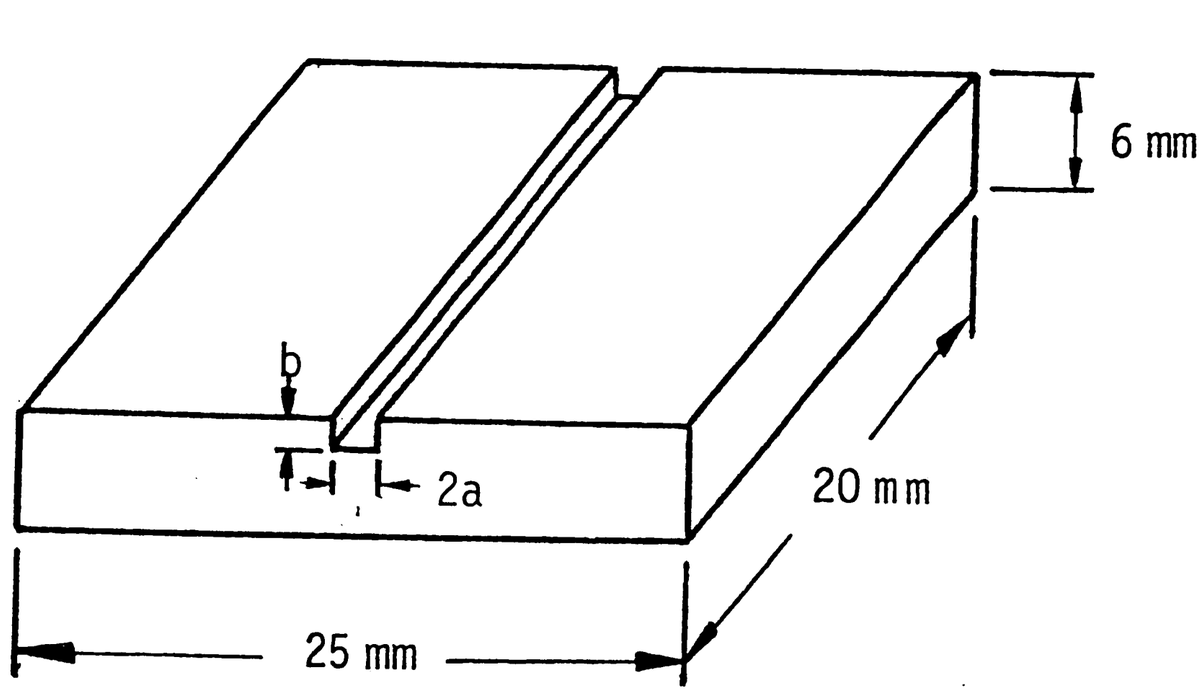

Figure 4 - Notch depths 1 and 2.

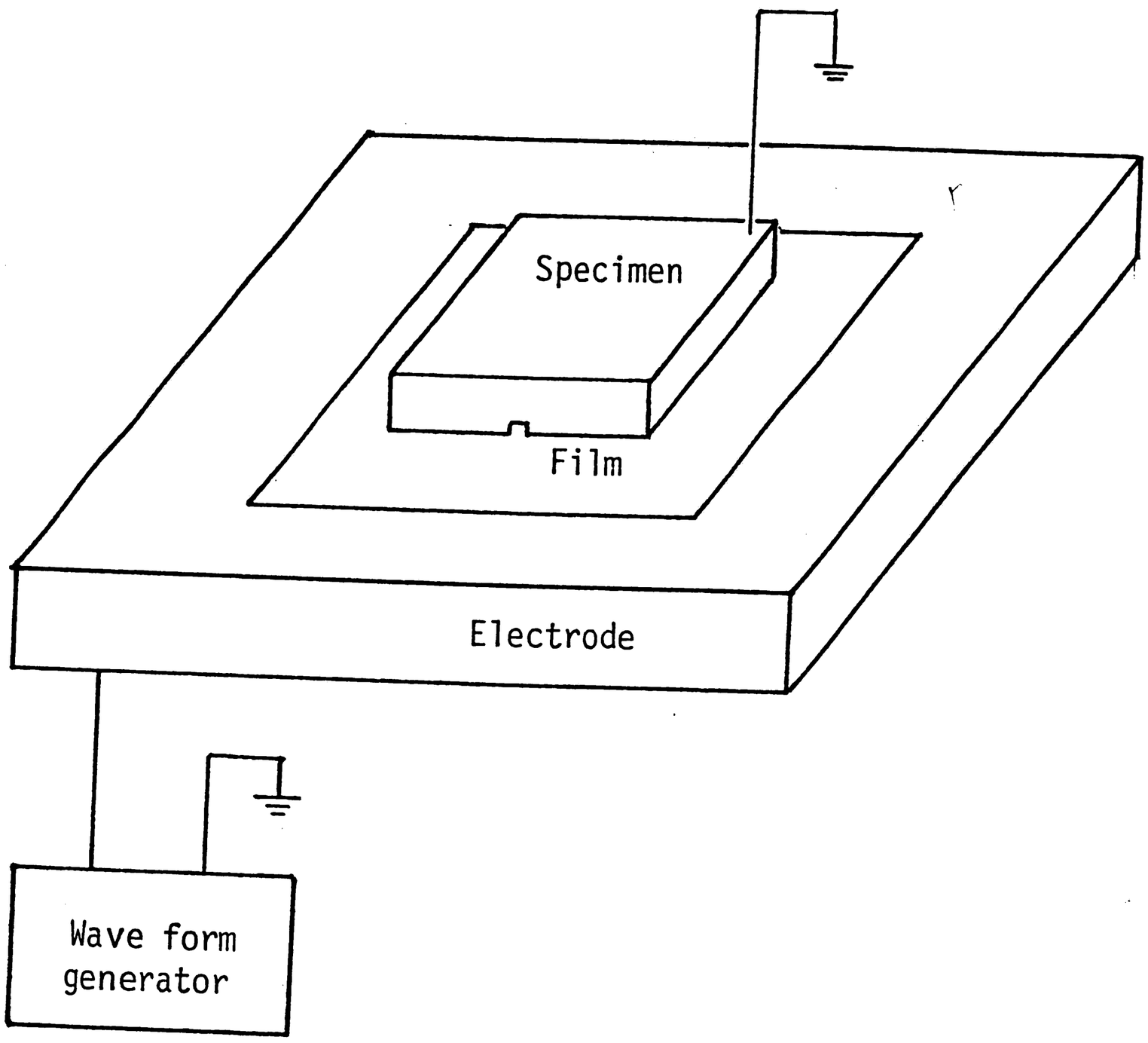

Figure 5 - Enlarged electrode specimen.

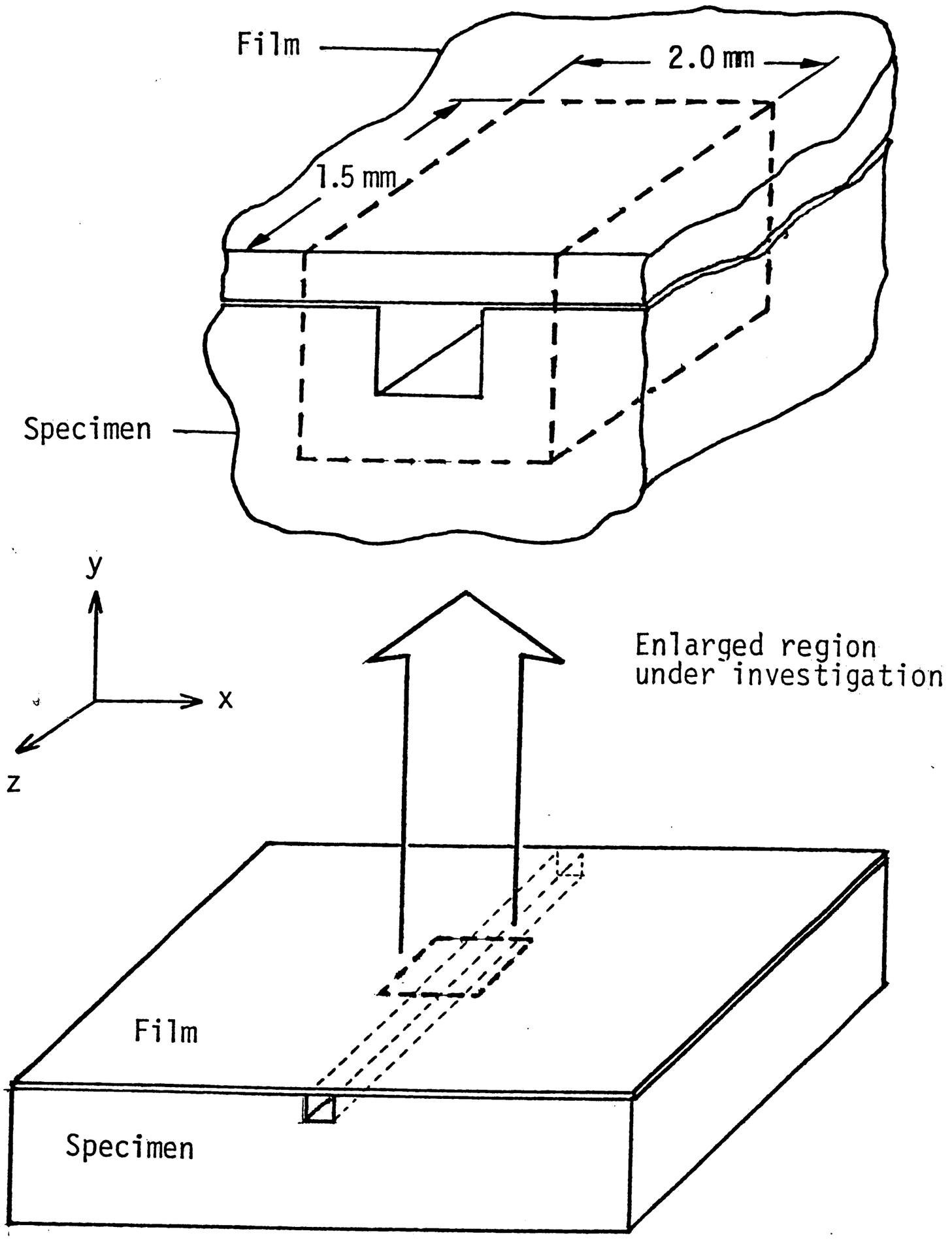

Figure 6 - Enlarged region from the middle of the notched surface.

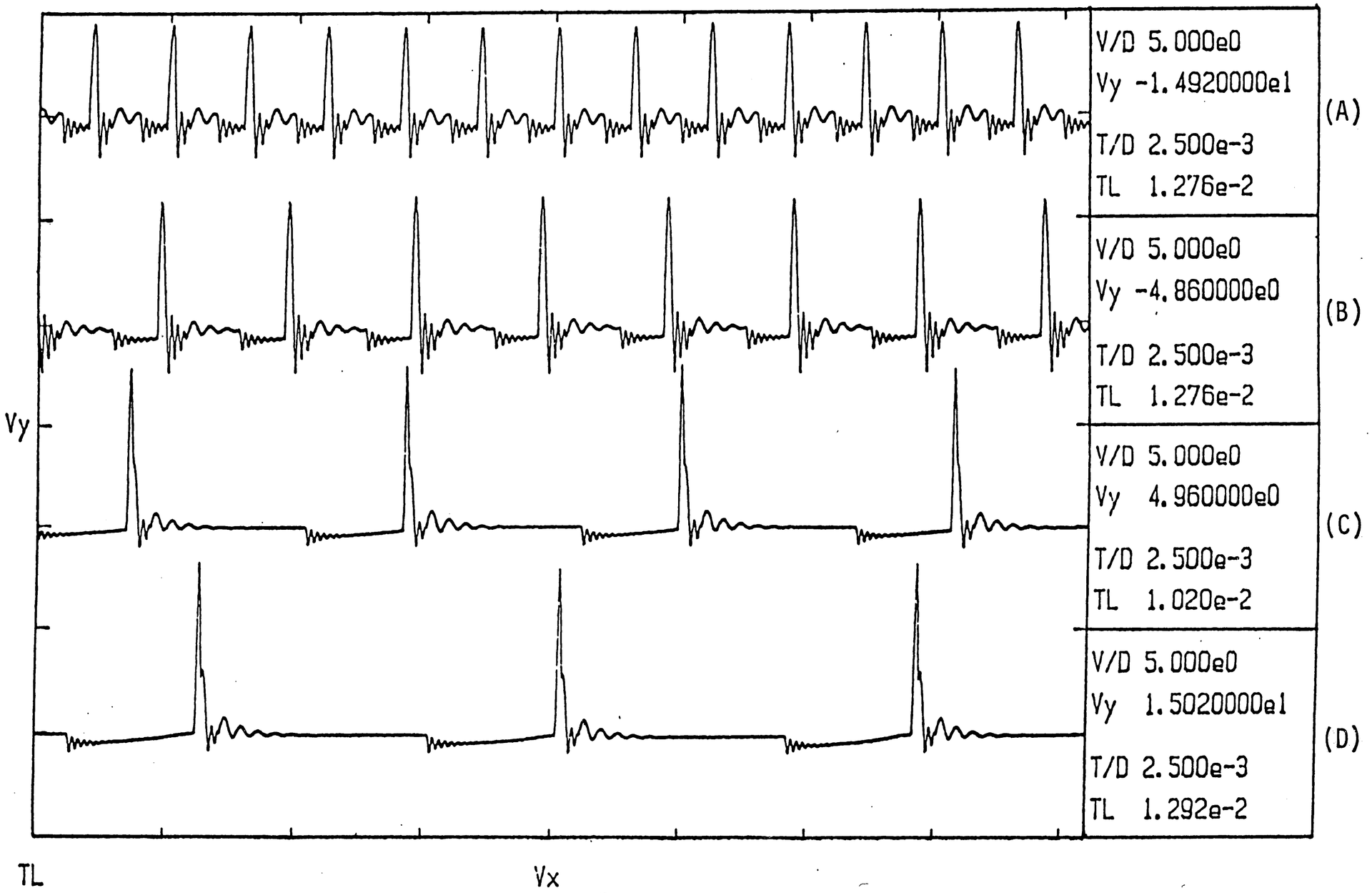

Figure 7 - Wave patterns at different excitation settings.

Table 1 - Pulse duration and peak-to-peak voltage of each wave packet at different excitation settings.

Excitation Setting	Pulse Duration T , m sec	Packet I		Packet II		Packet III	
		T1, μ sec	Peak-to-Peak Voltage, V	T2, μ sec	Peak-to-Peak Voltage, V	T3, μ sec	Peak-to-Peak Voltage, V
A	1.470	120	3800	315	425	115	650
B	2.415	185	6065	325	450	120	570
C	5.500	190	7975	315	500	120	605
D	6.890	200	4310	325	775	120	500

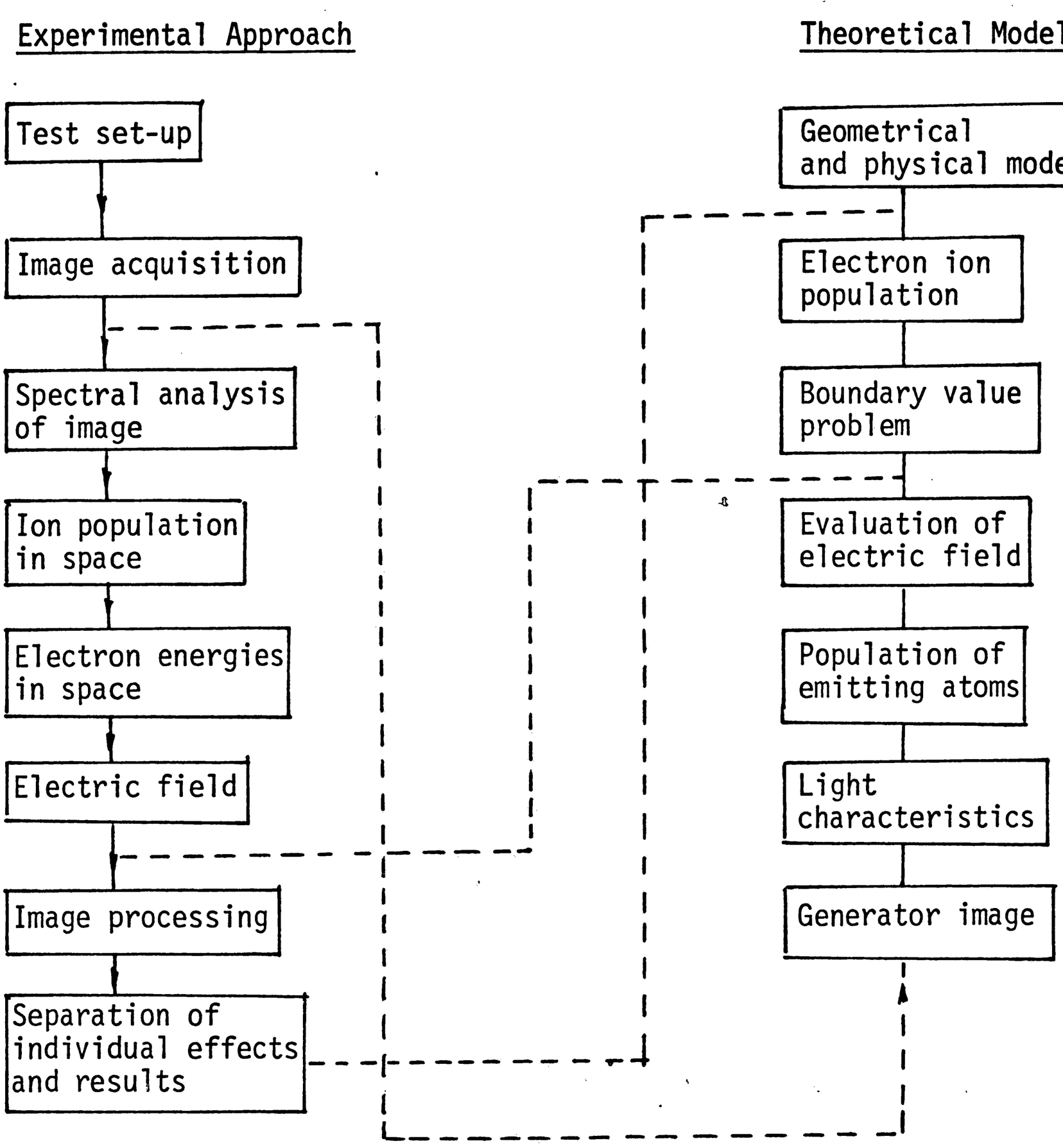

Figure 8 - Logic diagram of the EDI method: theory and experiment.

mentally. Physiochemical and geometrical effects will be included while the image will be processed digitally by the system [15] described in Figure 9. An image from the developed film is fed into the video camera. The image is then digitized and stored. Upon command from the job control input, the computer executes the image process program from a library and the output image is generated pixel by pixel. The results are written line by line on the output data storage device and the pixels may be modified at the discretion of the programer. Dedigitization is then made so that the image may be displayed visually. The gray level of each pixel determines the light intensity.

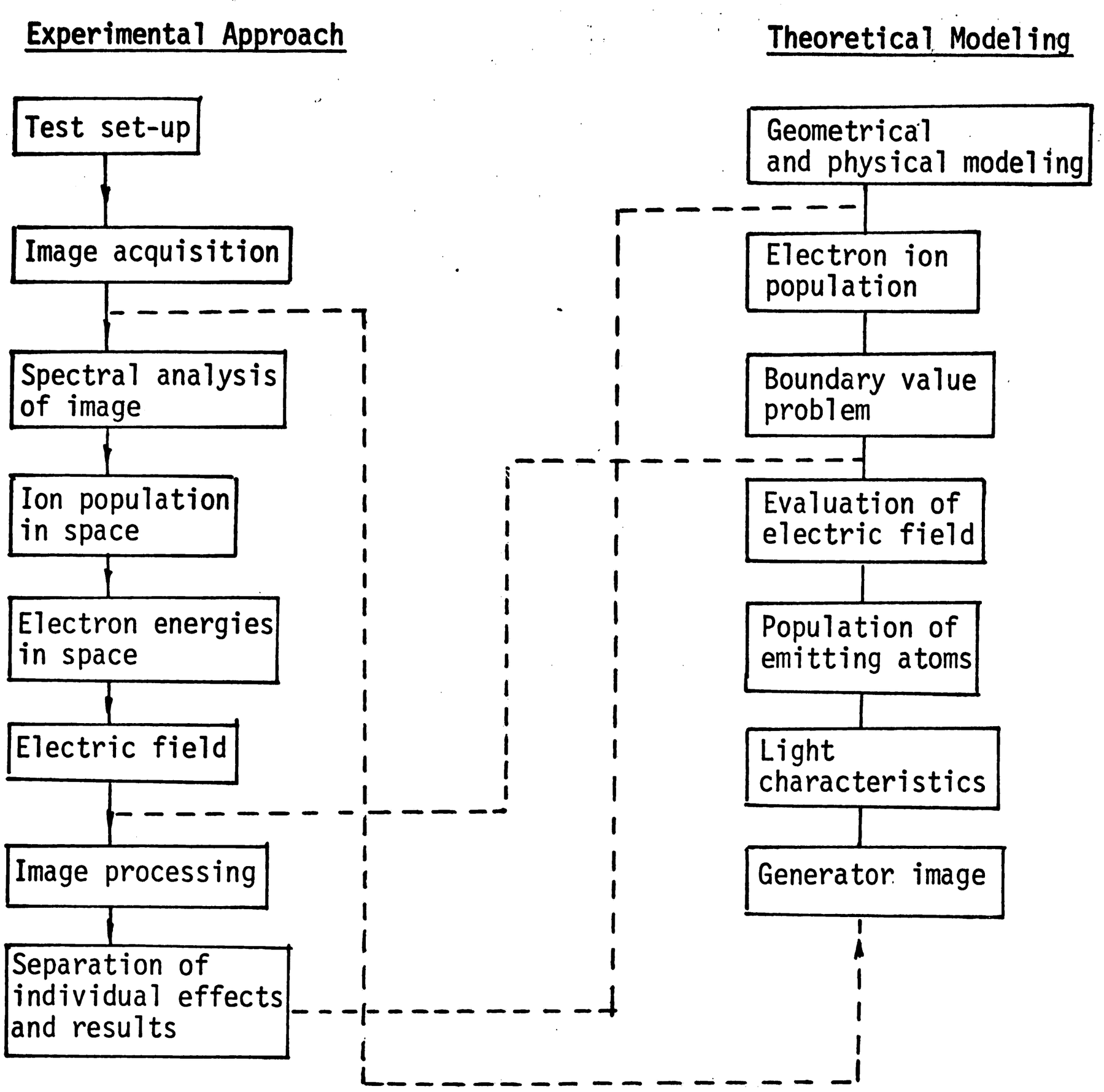

Figure 8 - Logic diagram of the EDI method: theory and experiment.

mentally. Physiochemical and geometrical effects will be included while the image will be processed digitally by the system [15] described in Figure 9. An image from the developed film is fed into the video camera. The image is then digitized and stored. Upon command from the job control input, the computer executes the image process program from a library and the output image is generated pixel by pixel. The results are written line by line on the output data storage device and the pixels may be modified at the discretion of the programer. Dedigitization is then made so that the image may be displayed visually. The gray level of each pixel determines the light intensity.

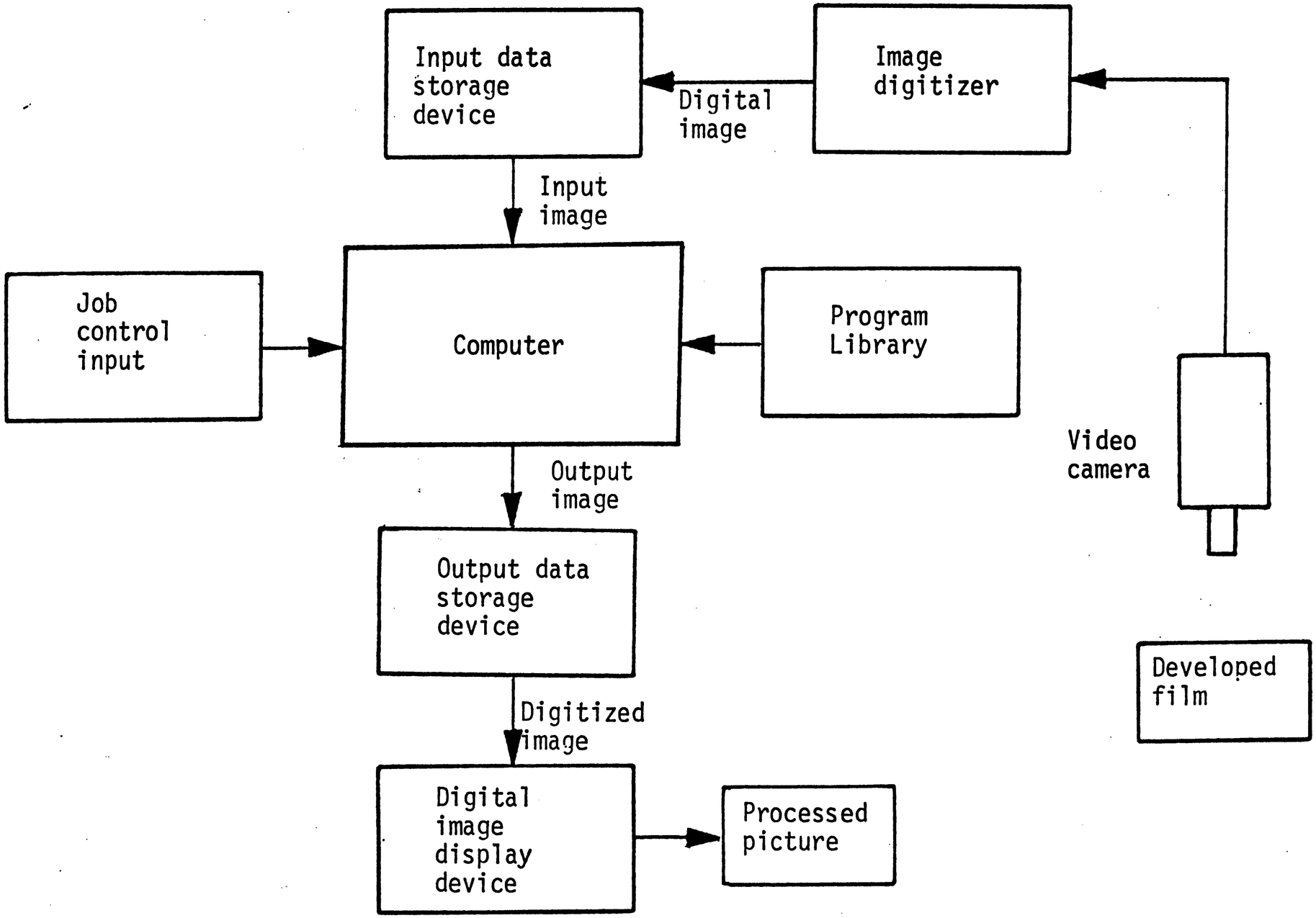

Figure 9 - Digital image processing flow chart.

CHAPTER IV - THEORETICAL CONSIDERATION

This section provides the theoretical background for predicting the EDI by using the notch specimen as the example while the underlying principle applies in general to any specimen configuration.

4.1 Description of Plasma Composition

Referring to the notch specimen configuration in Figure 10(a), a potential $V = V_1$ is applied to the electrode while the surface of the specimen indented by the notch is maintained at $V = V_o$. The plasma width corresponds to the distance d between the electrode and the specimen surface. If N_n, N_e and N_i denote, respectively, the density of the neutral atoms, electrons and ions, then the total gauge pressure P of the plasma can be written as

$$P = (N_n + N_e + N_i)kT \tag{1}$$

in which k is the Boltzmann constant and T the absolute temperature. The Saha equation [16] of ionization is given by

$$\frac{N_i N_e}{N_n} = S(T) \tag{2}$$

with the function S(T) defined as

$$S(T) = \frac{2g_i}{g_n} \left(\frac{2\pi mkT}{h^2}\right)^{3/2} \exp\left(-\frac{eV_i}{kT}\right) \tag{3}$$

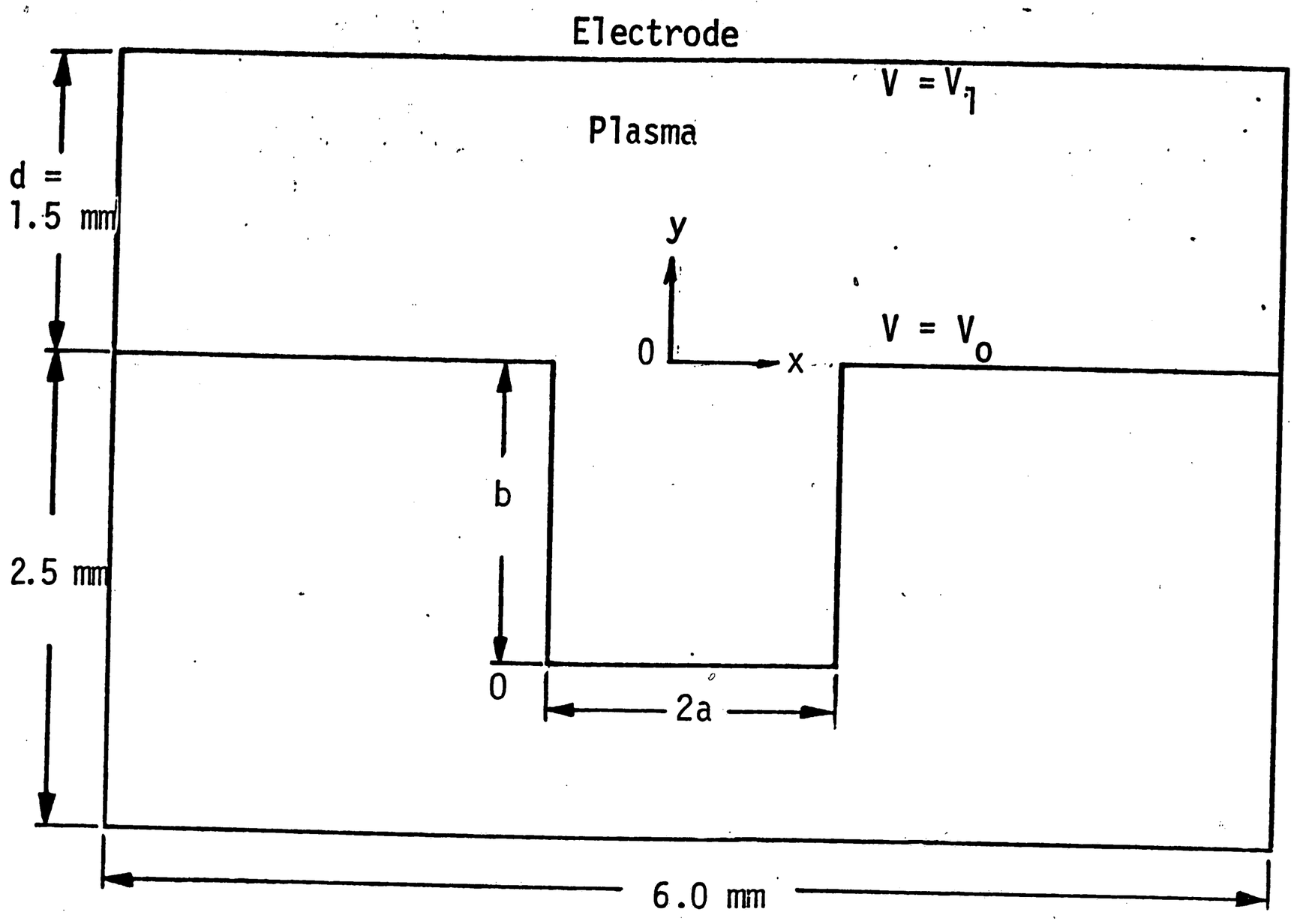

(a) Cross-section of the notch.

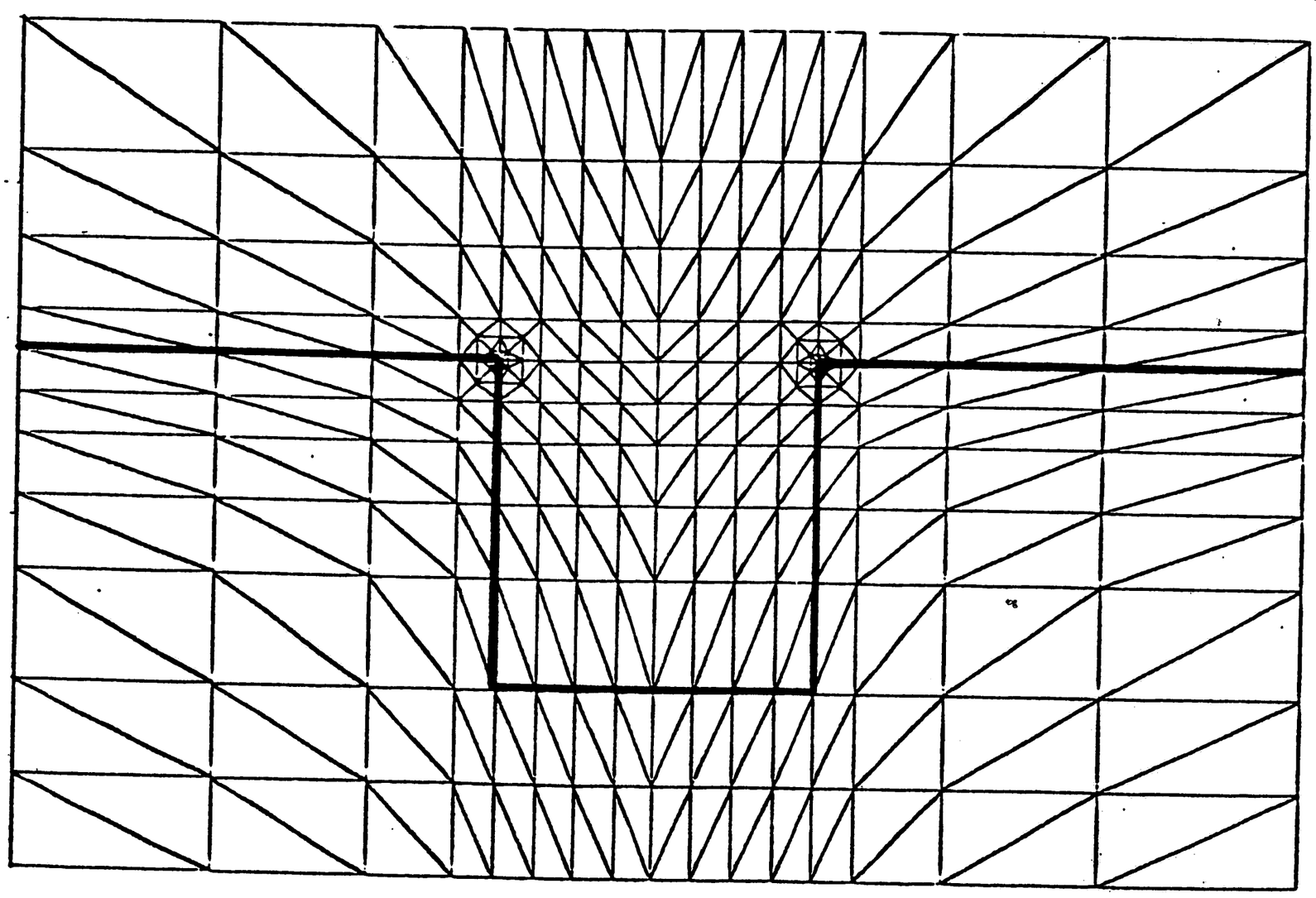

(b) Finite element grid pattern.

Figure 10 - Cross section of the notch and finite element grid pattern.

Here, g_i and g_n are the statistical weights of the ions and neutral atoms while m is the mass of an electron and h is the Planck constant. The ionization potential of the N_i ions is denoted by V_i.

The potential distribution V is governed by an equation of the form

$$\nabla^2 V = - \frac{\rho_o}{\varepsilon_o} \tag{4}$$

with ε_o being the permittivity of the medium under consideration and

$$\rho_o = e(\Delta N_e - \Delta N_i) \tag{5}$$

The parameter e stands for the electric charge. Use will be made of the Boltzmann equations [17]:

$$\Delta N_e = N_e[\exp(\frac{eV}{kT_e}) - 1] + N_e^* \tag{6}$$

and

$$\Delta N_i = N_i[\exp(\frac{eV}{kT_i}) - 1] \tag{7}$$

The densities of the electrons produced by the electrode are N_e^*. In equations (6) and (7), T_e and T_i are, respectively, the temperature associated with the electrons and ions. Now, because $eV/kT \ll 1$, both equations (6) and (7) may be approximated as

$$\Delta N_e \simeq N_e \left(\frac{eV}{kT_e}\right) + N_e^*, \quad \Delta N_i \simeq N_i \left(\frac{eV}{kT_e}\right) \tag{8}$$

In view of these considerations, equation (4) becomes

$$\nabla^2 V = - \frac{e^2}{k\varepsilon_o} \left(\frac{N_e}{T_e} - \frac{N_i}{T_i}\right) V - \frac{e}{\varepsilon_o} N_e^* \tag{9}$$

which is functionally of the form

$$\frac{N_e}{T_e} - \frac{N_i}{T_i} = f(V) \tag{10}$$

4.2 Electrode Process

Let v be the average velocity of the N_e^* electrons and I the electric current density. Hence

$$I^* = eN_e^* v \tag{11}$$

As the kinetic energy of an electron is acquired from the charged field, there prevails the relation

$$\frac{1}{2} mv^2 = eV \tag{12}$$

Substituting equation (12) into (11), there results

$$N_e^* = - I^* \sqrt{\frac{m}{2e^3 V}} \tag{13}$$

The current density I^* may be regarded as the sum of two components:

$$I^* = I_F + I_T \tag{14}$$

The thermionic current is given by [18,19]

$$I_T = AT^2 \exp(-\frac{\phi}{kT}) \tag{15}$$

where A is a constant having the dimension of current density.

Referring to the energy diagram in Figure 11, the potential energy of an electron is lower than that of the surrounding by an amount w. The kinetic energies are distributed with a maximum value ζ in accordance with the Fermi-Dirac statistics. The difference $(w-\zeta)$ is the work function ϕ of a metal in equation (15). It is the work required to remove an electron from the metal. The field emission current in equa-

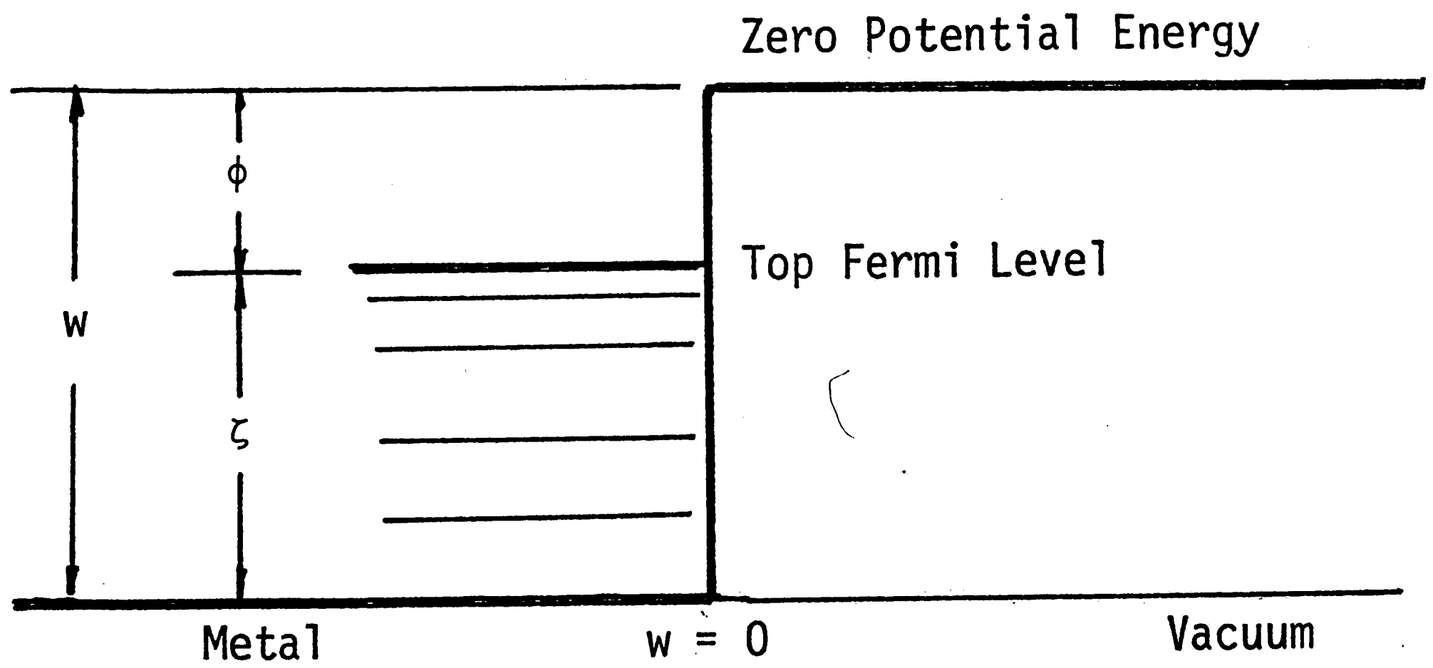

Figure 11 - Energy diagram of electrons in a metal.

tion (14) is [20]

$$I_F = \frac{38.5 \times 10^{12} \sqrt{\zeta} \Phi^2}{(\zeta+\phi)\sqrt{\phi}} \exp(-6.8 \times 10^7 \frac{\phi^{3/2}}{3\Phi}) \qquad (16)$$

in which Φ is the energy

$$\Phi = h\nu - \phi \qquad (17)$$

If $h\nu$ is the energy of a quantum of light and if $h\nu > \phi$, then an electron at the Fermi level could escape. In equation (17), ν is the frequency.

Substituting the sum of I_F and I_T for I^* in equation (13), N_e^* can be expressed in terms of the exponential functions involving ϕ, T, Φ, etc., and the result may be further inserted into the governing equation (9) for V. This gives a highly nonlinear differential equation that can only be solved numerically.

A finite element procedure was used, the details of which are beyond the scope of this investigation. The grid pattern containing 416 triangular elements and 236 nodes is shown in Figure 10(b). Refinement of the meshes near the corners at the entrance of the notch is made in order to improve the accuracy of the local solution. Typical contours of the electric potential and field intensity are shown, respectively, in Figures 12(a) and 12(b).

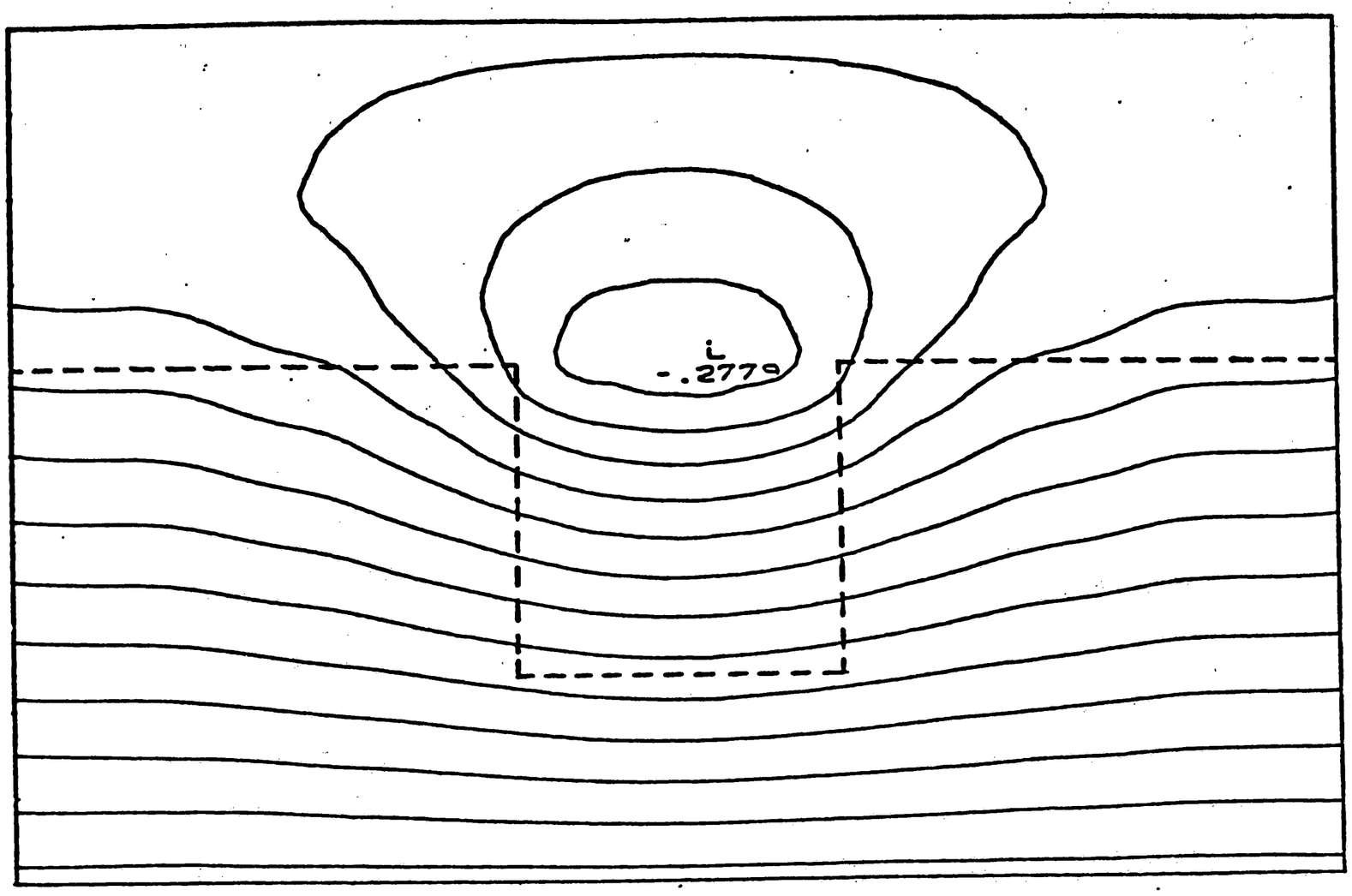

(a) Electric potential contour.

(b) Electric field intensity contour.

Figure 12 - Electric potential and field intensity contours.

4.3 Plasma Spectrum Analysis

The sources of continuous radiation in plasmas are transitions of free electrons into lower energy free states or bound states. The intensity is proportional to the product of the densities of ions N_i and electrons N_e and the line intensities. If ΔU^* is the energy differential of the upper level from that of ionization, then the corresponding power dH radiated in a spectral line by a small volume element $d\tau$ is

$$dH = \frac{8\pi^2 h\nu^3 e^2}{mc^2} \frac{g^*}{2g_i} \left(\frac{h^2}{2\pi mkT}\right)^{3/2} G_a \exp\left(\frac{\Delta U^*}{kT}\right) N_i N_e d\tau \qquad (18)$$

in which m is the mass, c the light velocity and G_a the absorption oscillator strength. In equation (18),

$$\Delta U^* = \frac{eV_i}{n^2} - h\nu \qquad (19)$$

with n being the number of electrons. Making use of equation (18), the intensity J is defined:

$$J = \frac{dH}{d\tau} \qquad (20)$$

For emission spectroscopy, it is more convenient to use the relation

$$kT_e = \frac{h(\nu_1 - \nu_2)}{\log(J_2/J_1)} \qquad (21)$$

As an example, the intensity ratios of the hydrogen continuum is plotted in Figure 13. The process can be described by interactions in-

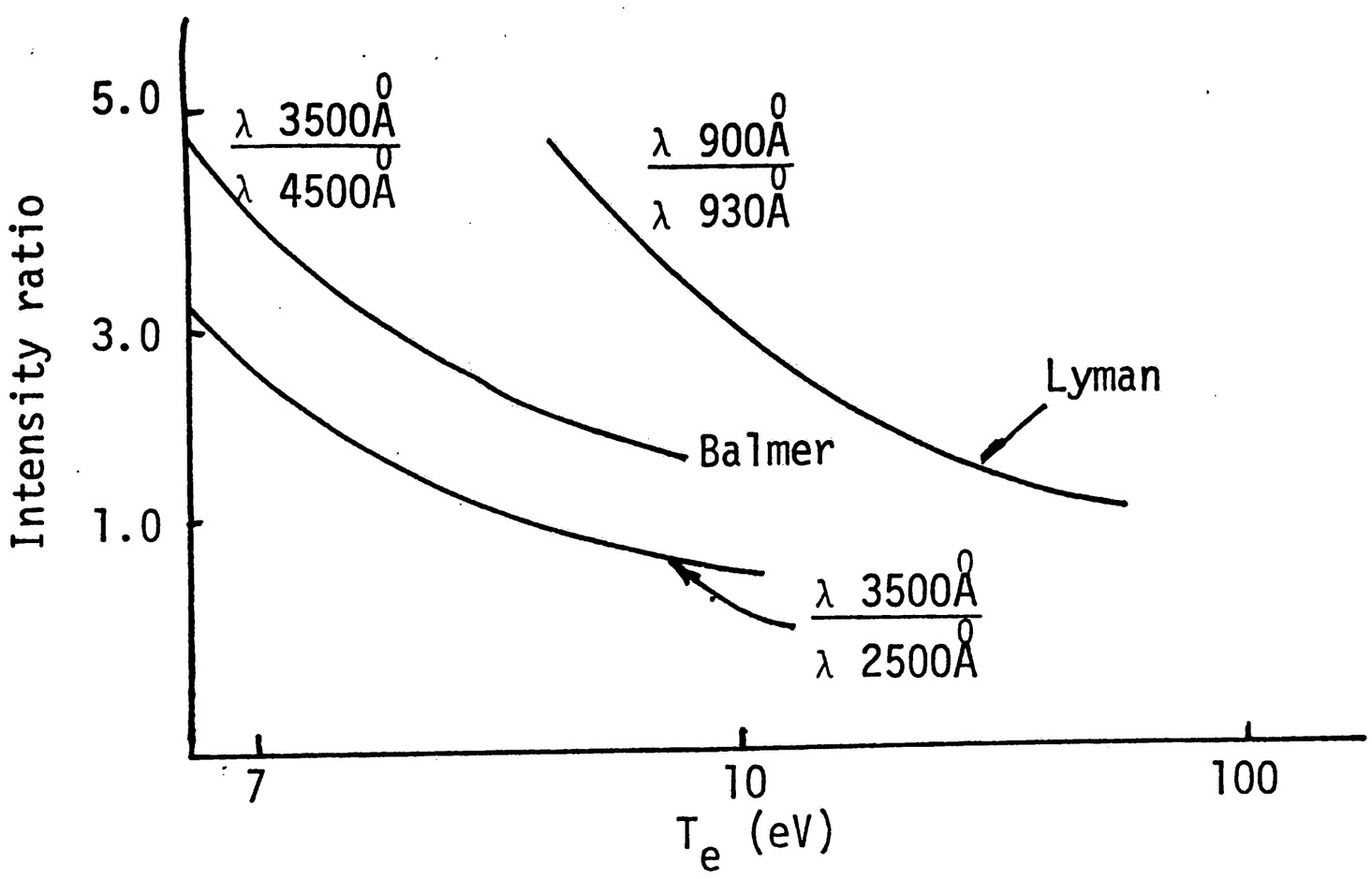

Figure 13. Variations of intensity ratio with temperature.

volving the nitrogen and oxygen:

$$N_2 + e^- \rightarrow N_2^+ + e^- + e^{-*}$$

$$O + e^{-*} \rightarrow O^* + e^-$$

$$N_2^* + e^- \rightarrow N_2^* + h\nu_1 \qquad (22)$$

$$N_2^* \rightarrow N_2 + h\nu_2$$

$$O^* \rightarrow O + h\nu_3$$

The energy of the photons for the visible spectrum (400 - 700 nm) is between 3.15 eV and 1.8 eV for colors from violet to red.

Excitation in an atom can be created by electric, thermal and/or light disturbance. The absorbed energy drives an atom from the ground state to one of the quantum levels. This is because an electron tends to go to the next higher orbital. It can arrest at one of the intermediate orbitals when returning to initial orbital. Radiation $h\nu$ is thus emitted equivalent to the partial quantum level of the corresponding orbital.

The mechanical, physical and chemical variations in the specimen are contained in the image. These effects are reflected by equation (18) via the quantities: ν, g_i, g^*, T, G_a, ΔU^*, N_i and N_e. By application of pixel classification techniques, each one of the aforementioned effects can be isolated.

CHAPTER V - DISCUSSION OF RESULTS

All the EDI experiments were carried out in a dark room such that the notched surface was firmly in contact with the emulsion side of the film. The wave form generator was set to drive for 0.1 second while the film was exposed for the same period of time. A series of pictures were taken for each specimen with excitation settings A, B, C and D as defined in Table 1. The information collected on the developed film was then digitized by the process described in Figure 9. Computer processing of the light intensity distribution was then made and the results were compared with those predicted analytically from equation (19).

5.1 Electric and Light Field Intensity

The electric field intensity denoted by E is given by

$$E = -\text{grad } V \tag{23}$$

in which V is obtainable numerically by solving equation (9). It is also proportional to the light field intensity J depending on the frequency. Figure 14(a) and 14(b) give the topological plots of E and J, respectively, in the vicinity of notch 1. The experimentally measured J corresponds to excitation setting A. While the general features of the E and J surface are similar in that they tend to dip at the bottom of the notch, the edge effects detected experimentally in Figure 14(b) did not show up numerically in Figure 14(a). This is to be expected as

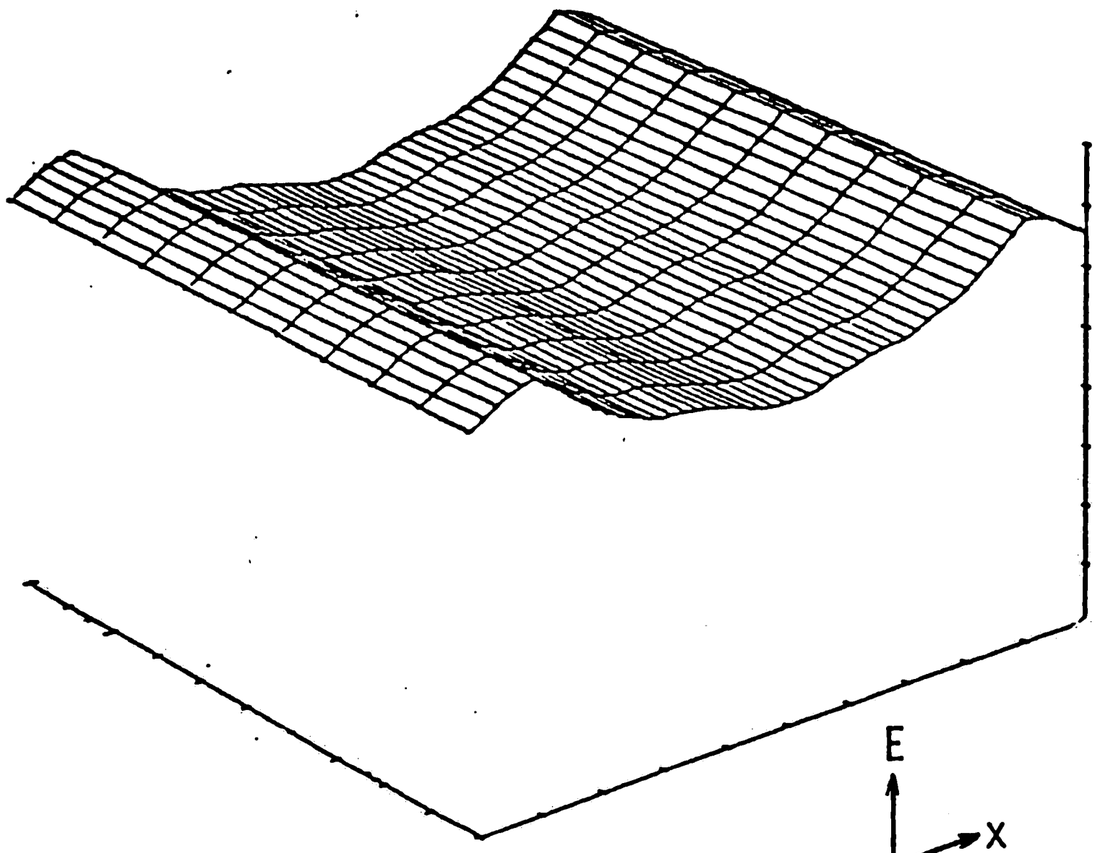

(a) Spacial distribution of electric field intensity.

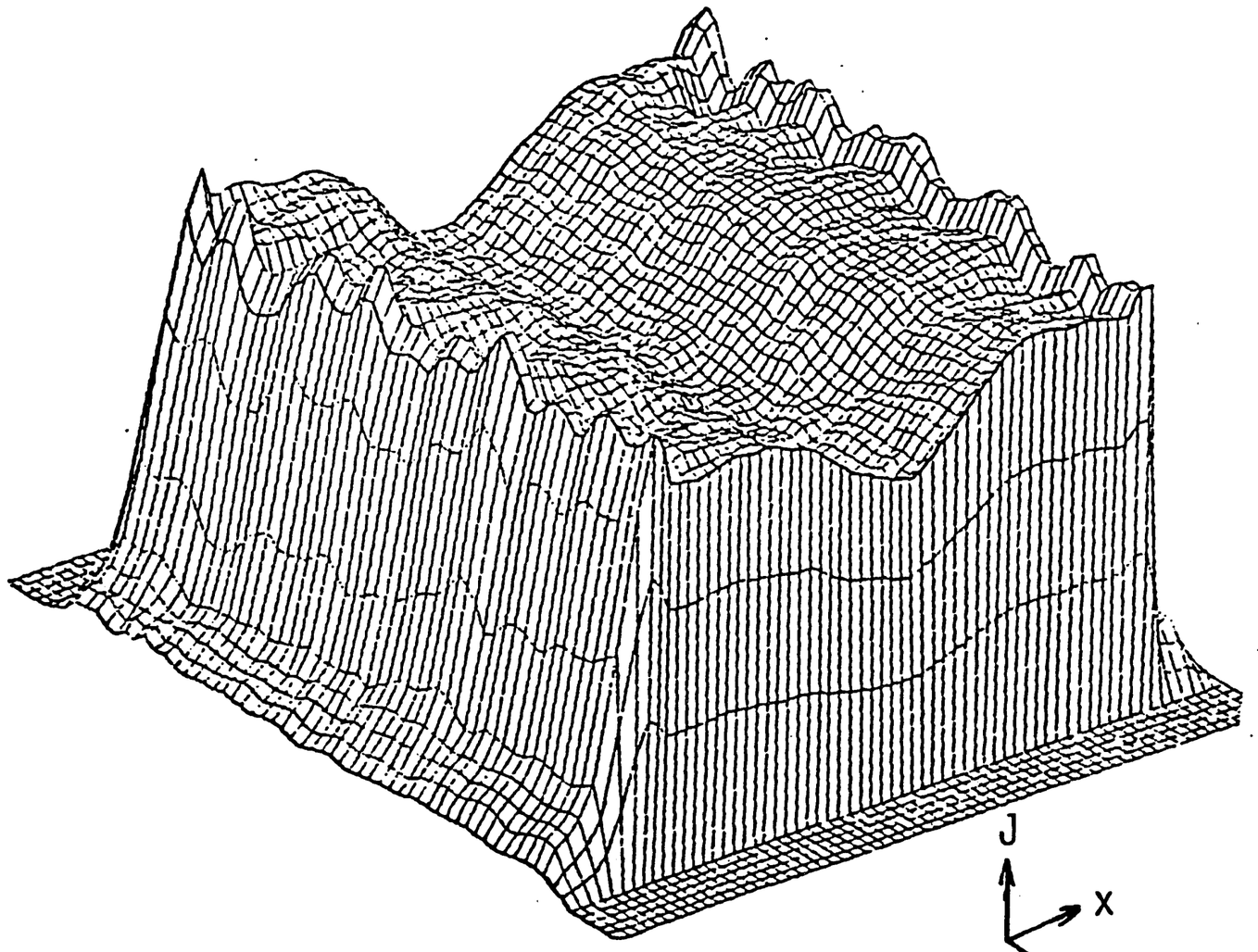

(b) Spacial distribution of light field intensity for excitation A.

Figure 14 - Electric and light field intensity distribution for Notch 1.

the finite element calculations normally do not capture the local effects unless special consideration is given. Similar plots of E and J are displayed in Figure 15 for notch 2 whose depth is one-half of that of notch 1. The corresponding amplitudes of E and J are also seen to be smaller.

The influence of the excitation settings on the J surface is shown by the computer plots in Figures 16 to 19 inclusive. The notch depth effect is most pronounced for excitation setting A. According to the results in Figure 16(a) for notch 1 and Figure 16(b) for notch 2, the J intensity is directly proportional to notch depth. This effect is not so visible for excitation settings of B, C and D in Figures 17 to 19.

5.2 Average Intensities

The results in Figures 14 to 19 inclusive can be best illustrated by averaging them along the notch length of 20 mm such that E and J can be plotted in a two-dimensional space as a function of x in the range $-0.75 \text{ mm} \leq x \leq +0.75 \text{ mm}$. Shown in Figure 20 is the theoretical prediction of E versus x. Note that the curve for notch 1 dipped lower than that for notch 2 and they both intersected at $x \simeq \pm 0.4$ mm. This trend will be compared with the experimental data on J.

Shown graphically in Figure 21 are the light intensity data for the two notches excited in accordance with setting A. Indeed, the general trend is similar to the theoretical prediction in Figure 20 except the curves intersected a number of locations and are not symmet-

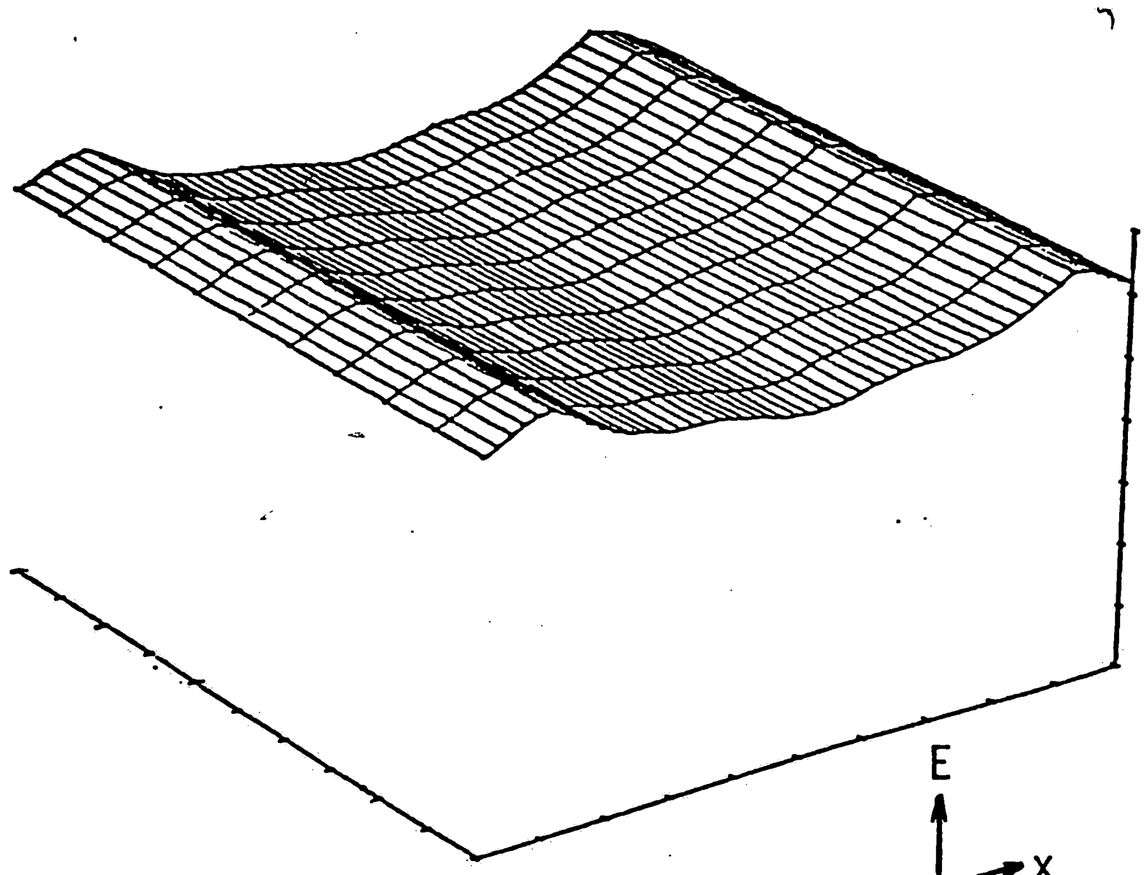

(a) Spacial distribution of electric field intensity.

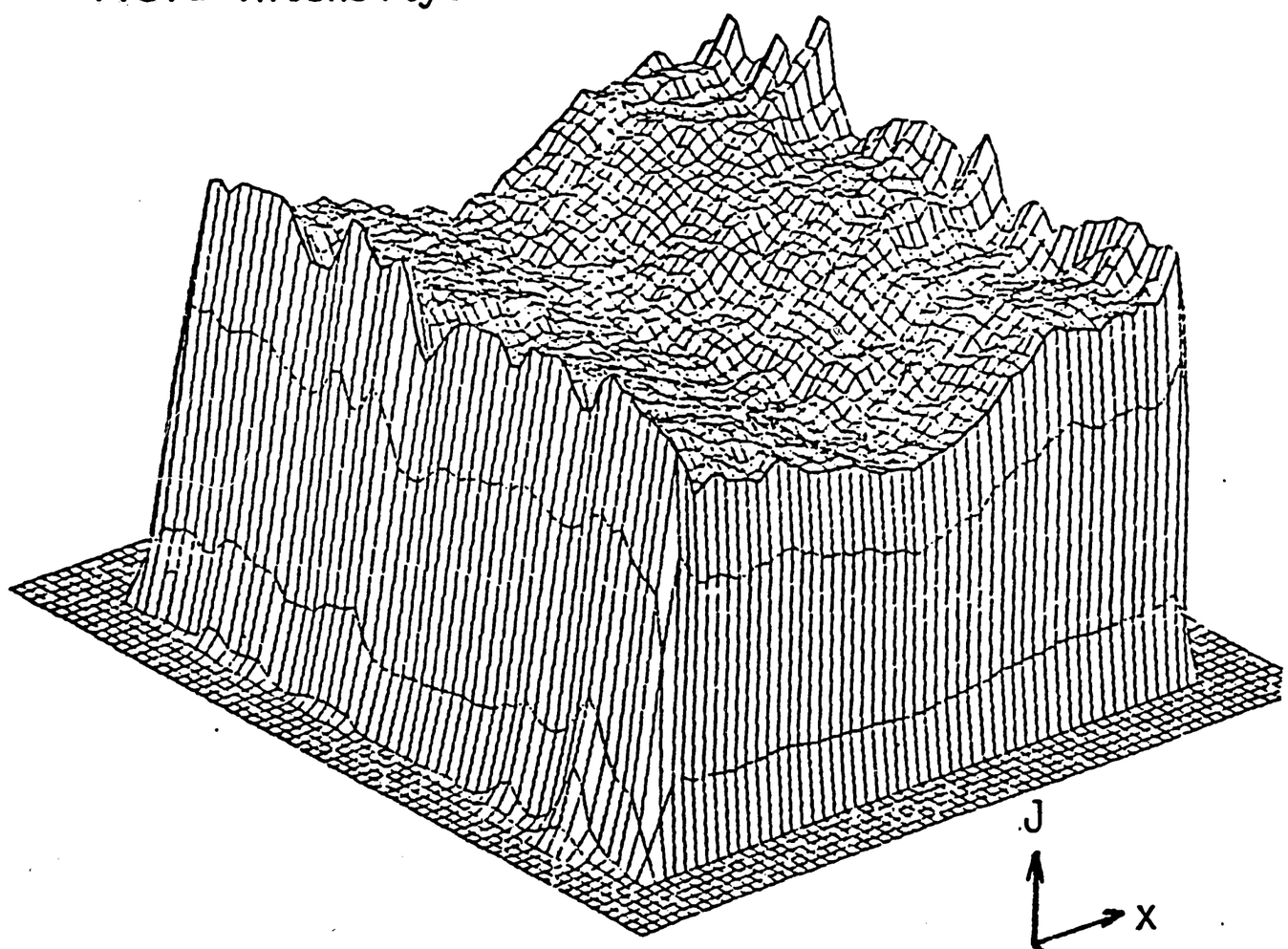

(b) Spacial distribution of light field intensity for excitation A.

Figure 15 - Electric and light field intensity distribution for Notch 2.

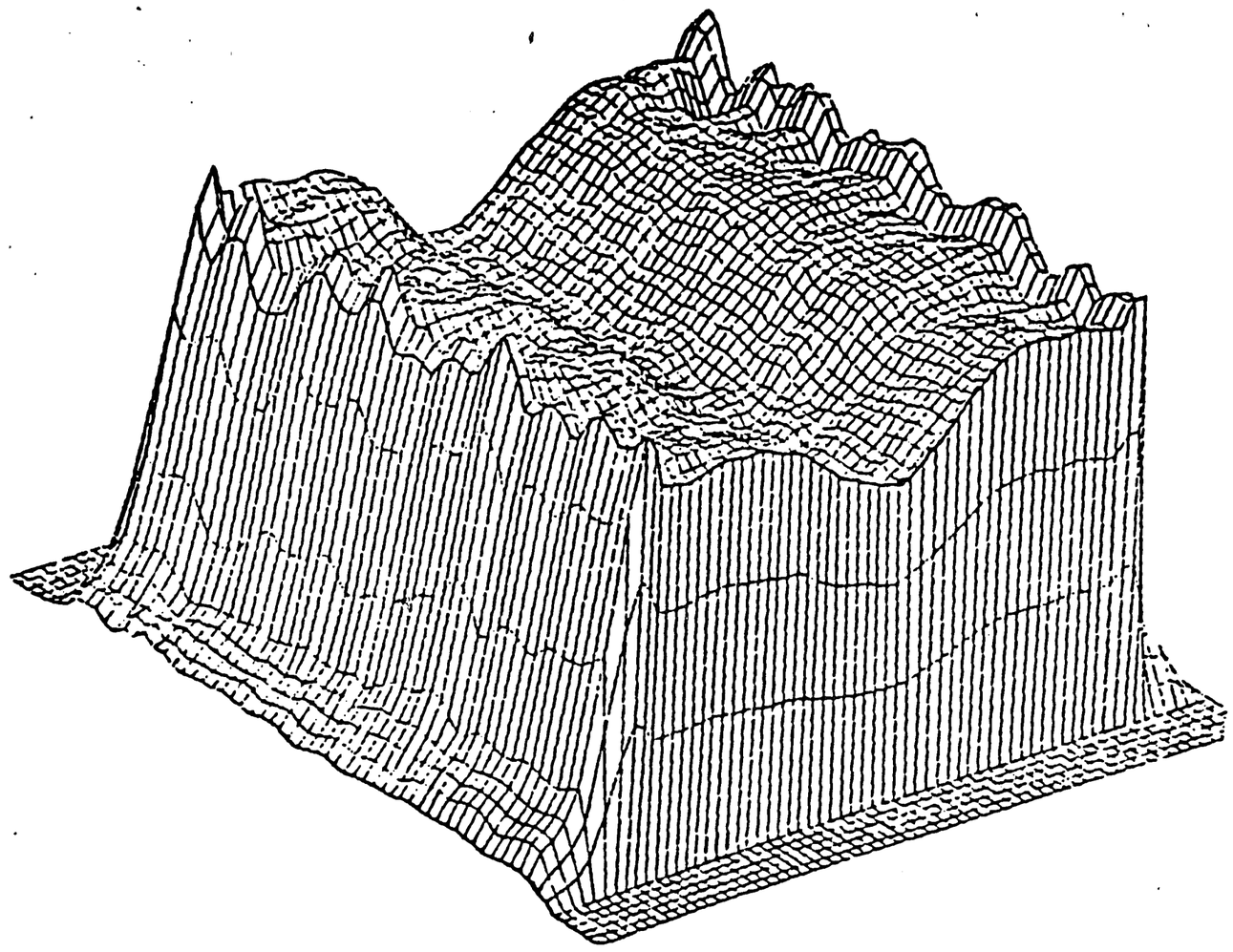

(a) Notch 1

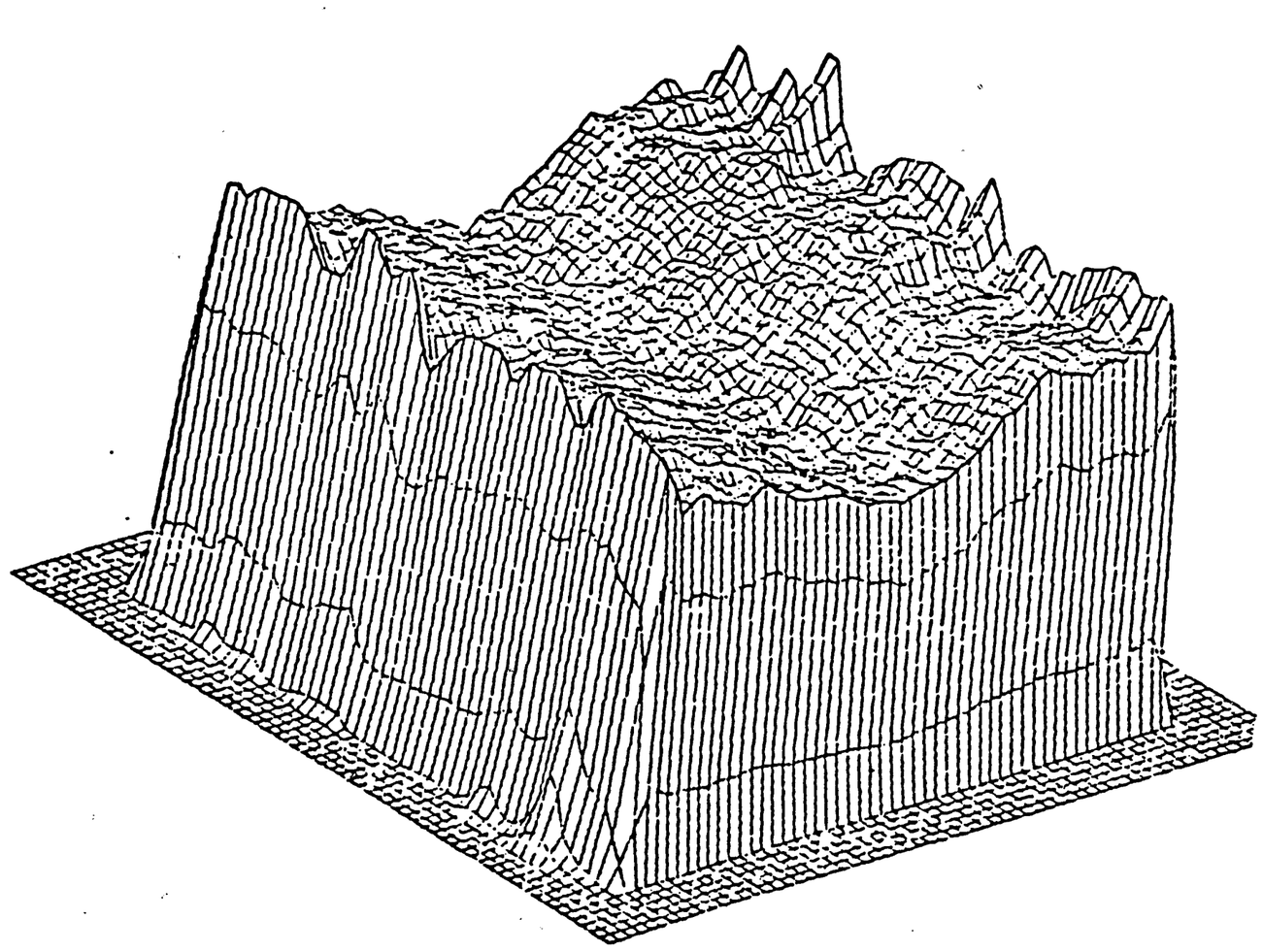

(b) Notch 2

Figure 16 - Comparison of light intensity distribution of Notch 1 and 2 at excitation A.

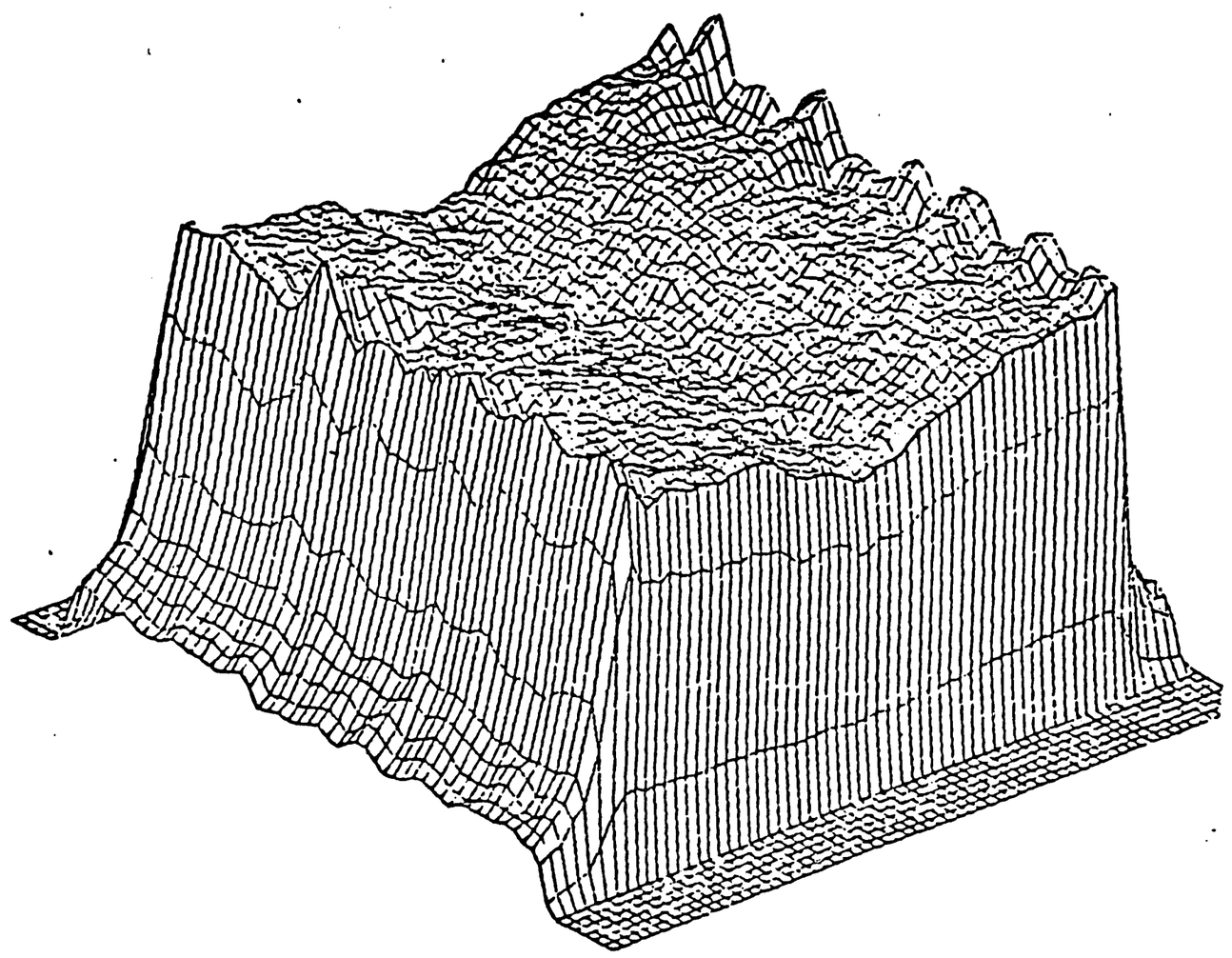

(a) Notch 1

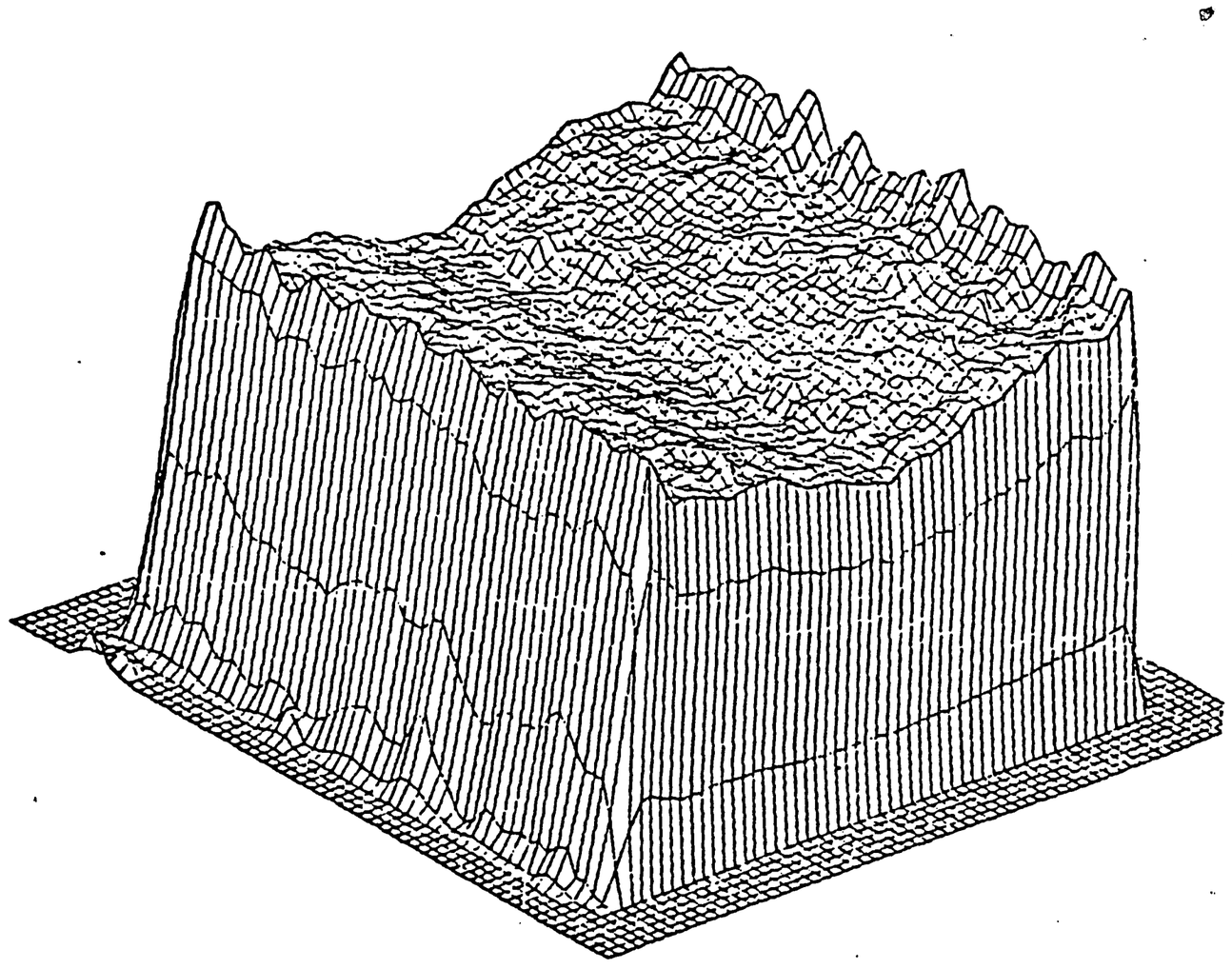

(b) Notch 2

Figure 17 - Comparison of light intensity distribution of Notch 1 and 2 at excitation B.

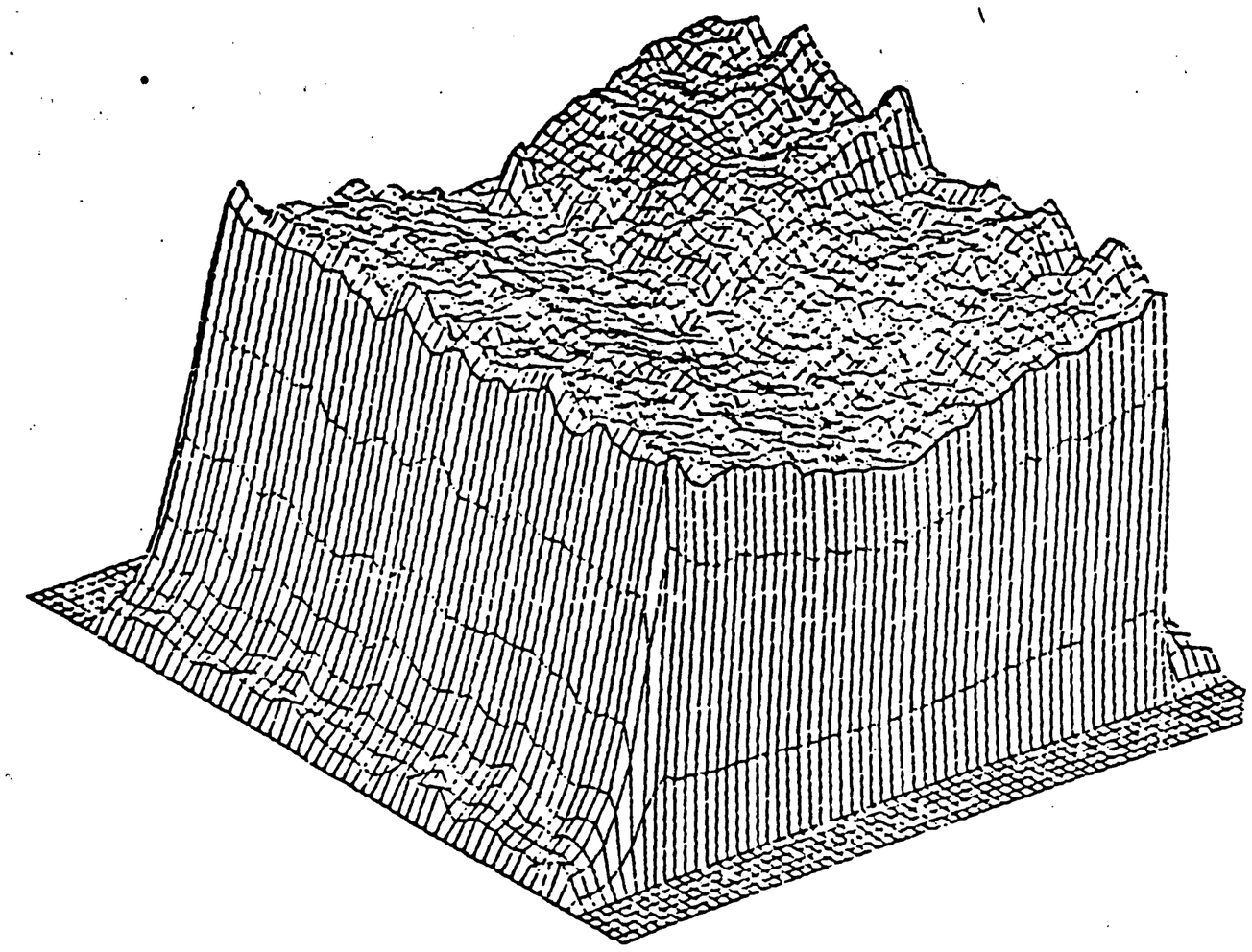

(a) Notch 1

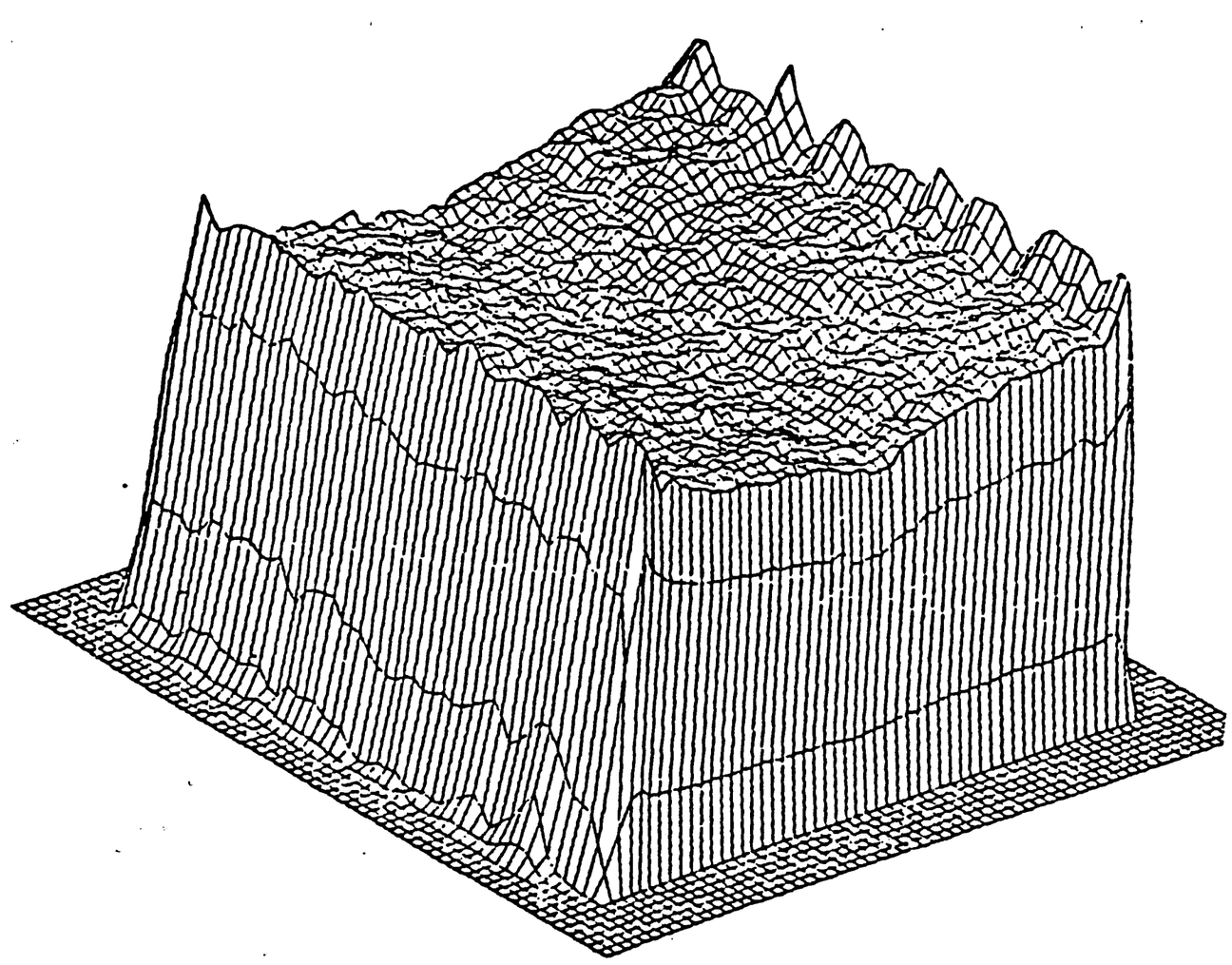

(b) Notch 2

Figure 18 - Comparison of light intensity distribution of Notch 1 and 2 at excitation C.

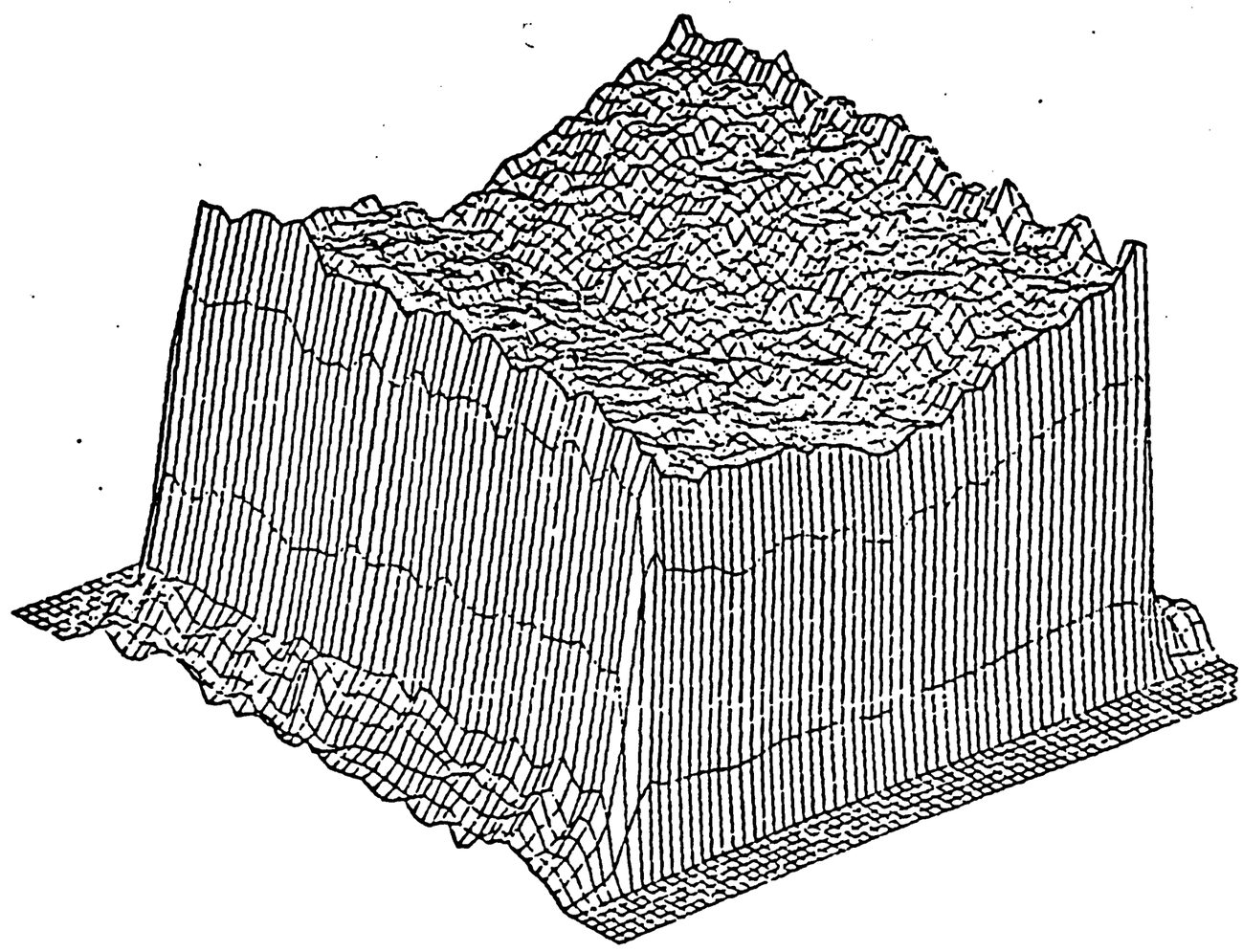

(a) Notch 1

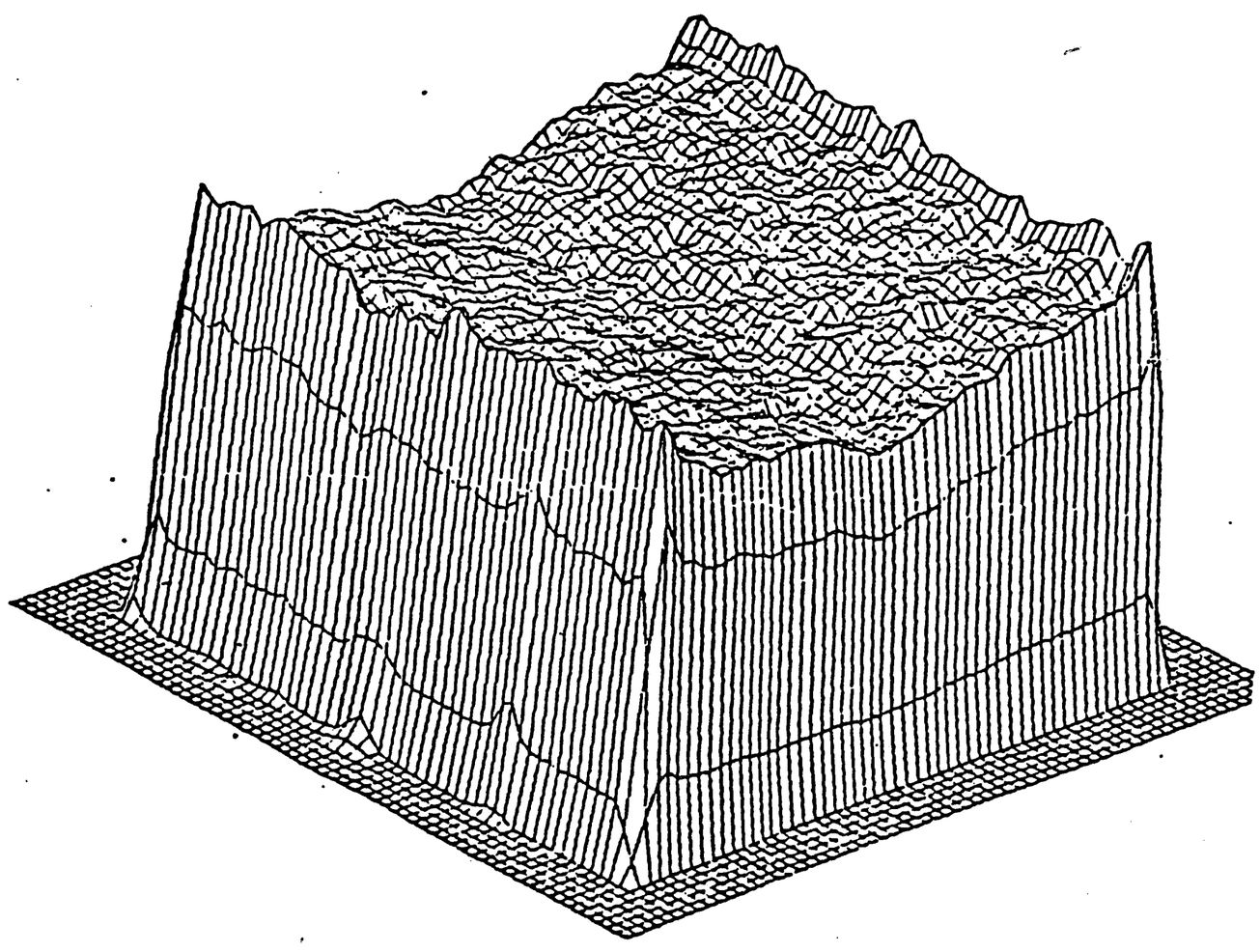

(b) Notch 2

Figure 19 - Comparison of light intensity distribution of Notch 1 and 2 at excitation D.

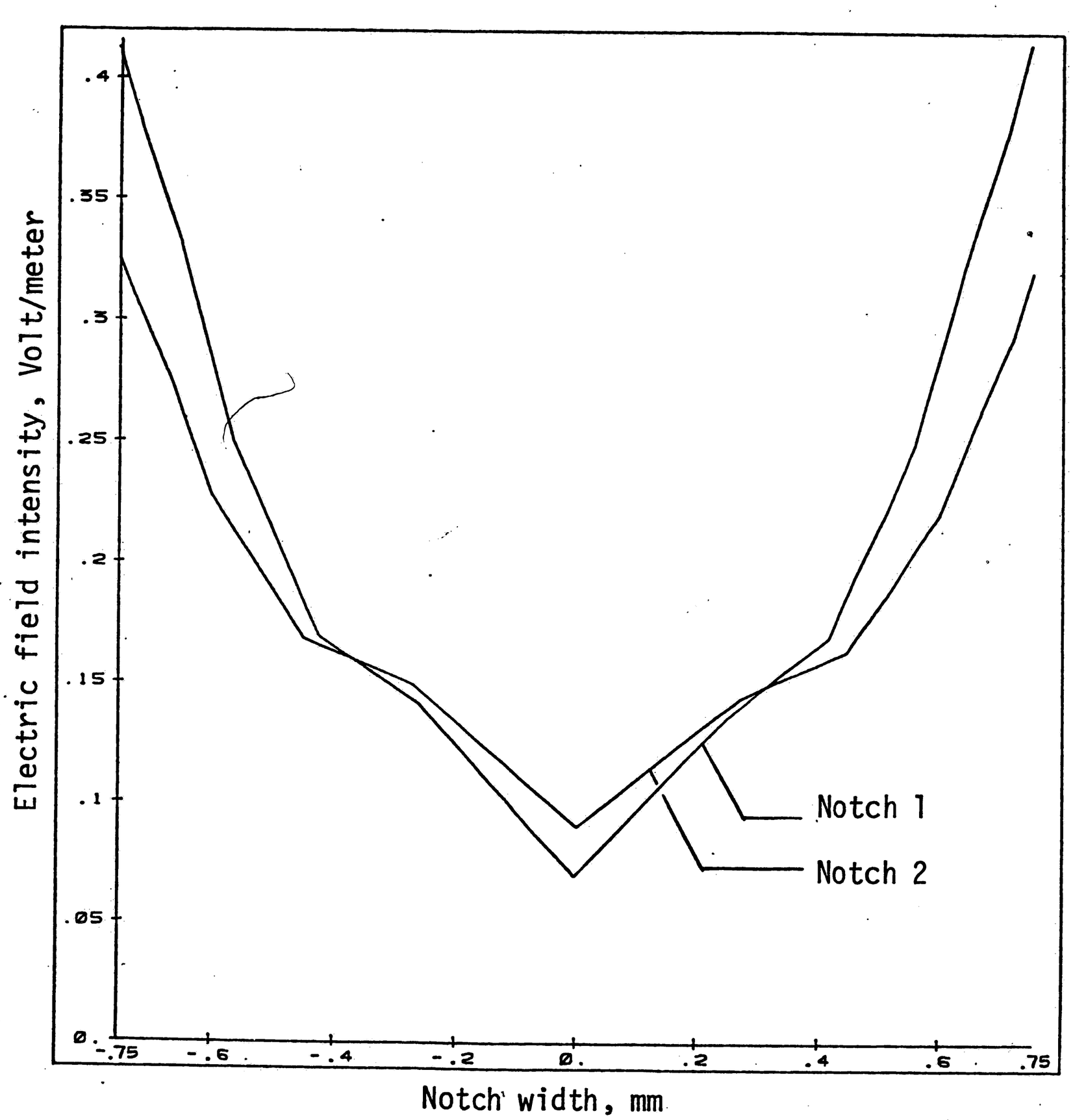

Figure 20 - Electric field intensity on film boundary and air gap for Notches 1 and 2.

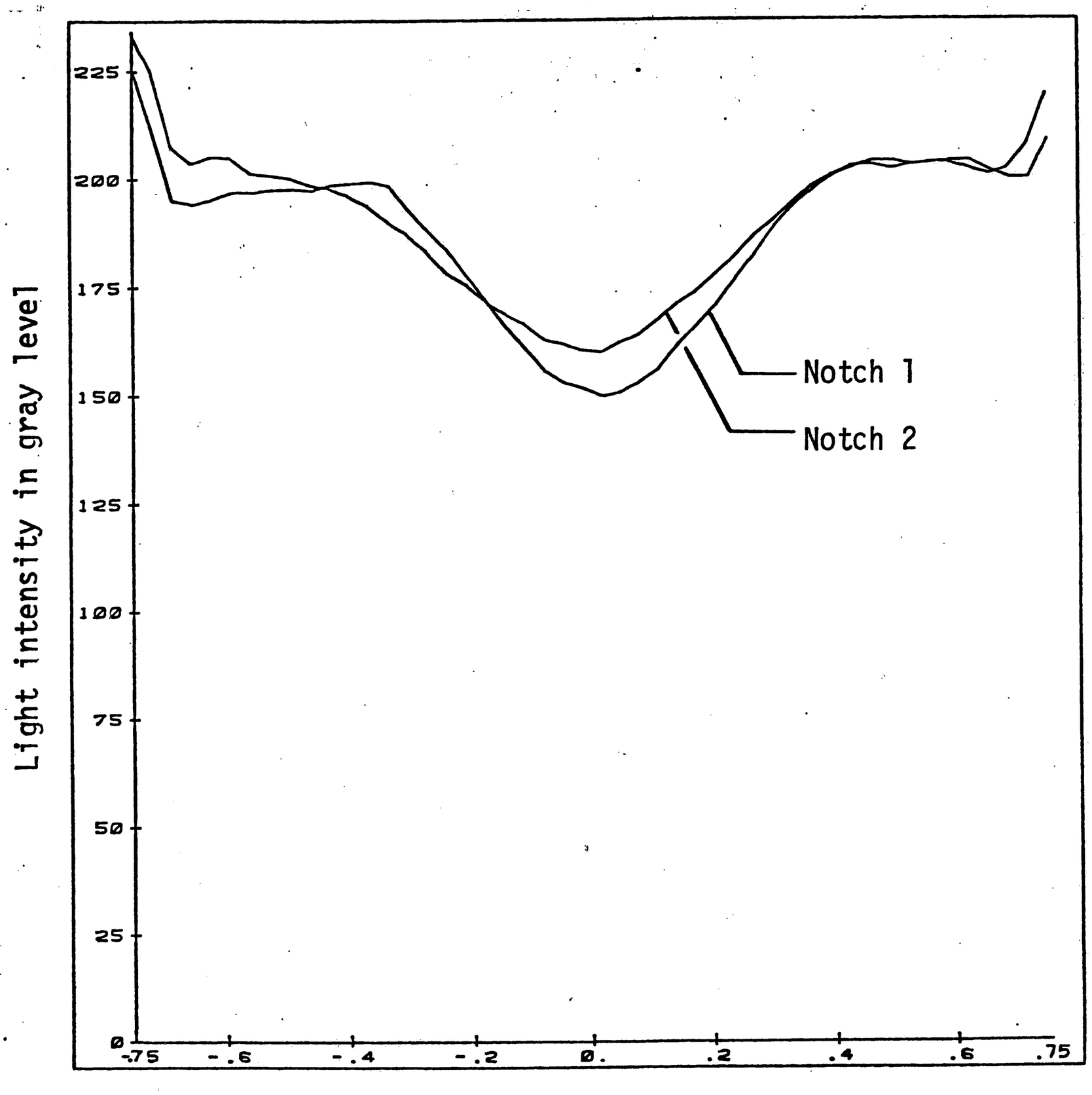

Figure 21 - Light intensity over notch region for Notches 1 and 2 at excitation A.

rical about the centroidal geometric axis x = 0 of the specimen. This is because the EDI process is sensitive to any mechanical, thermal and electrical variations that prevail in the specimen. Such effects, of course, are not modelled in the theoretical analysis. The J distributions corresponding to excitation settings B, C and D are given in Figures 22 to 24. They do not exhibit good correlation with change in notch depth. Summarized in Figures 25 and 26 are the J versus x variations for notch 1 and 2 where the effects of the four excitations are compared.

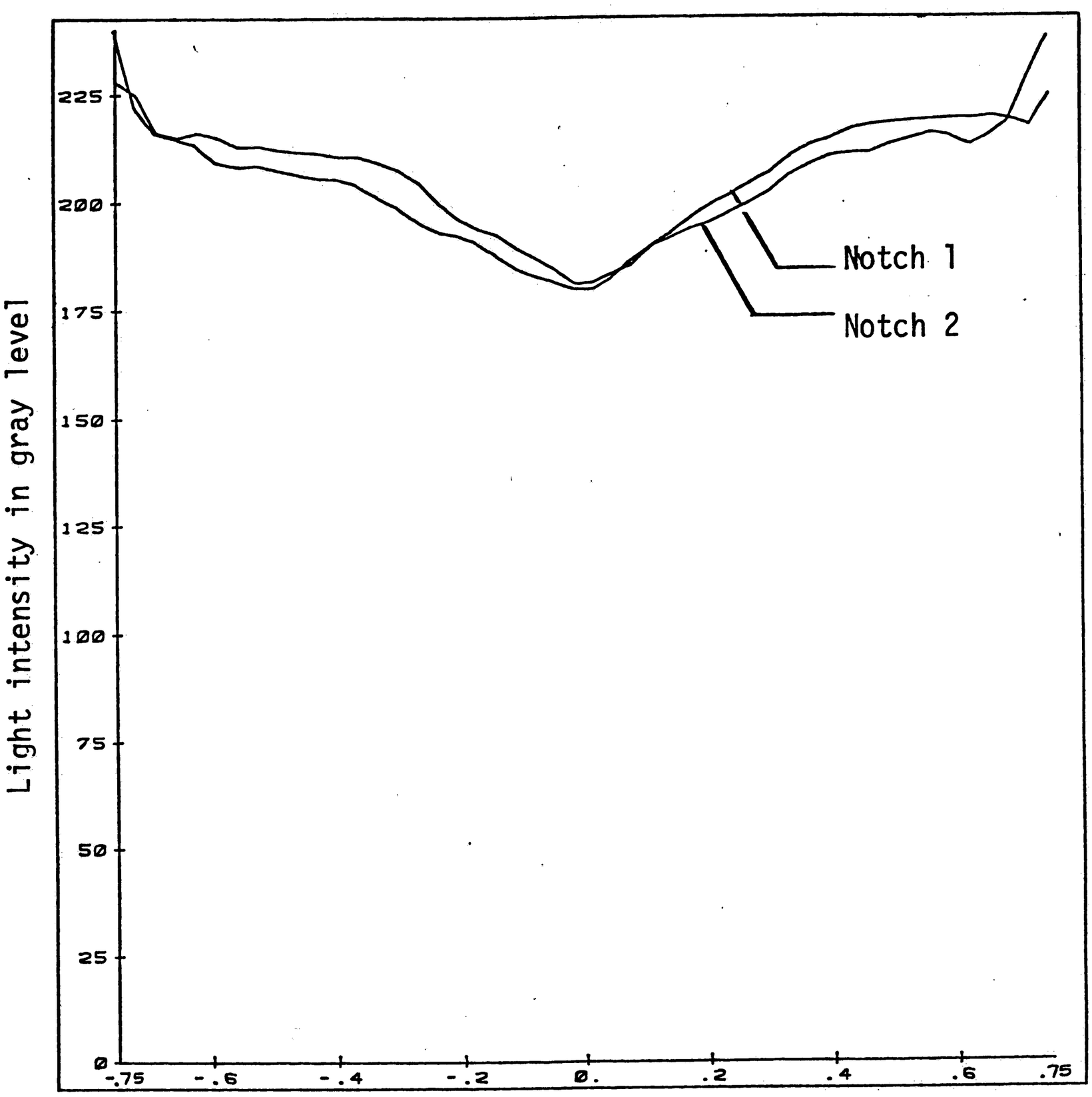

Figure 22 - Light intensity over notch region for Notches 1 and 2 at excitation B.

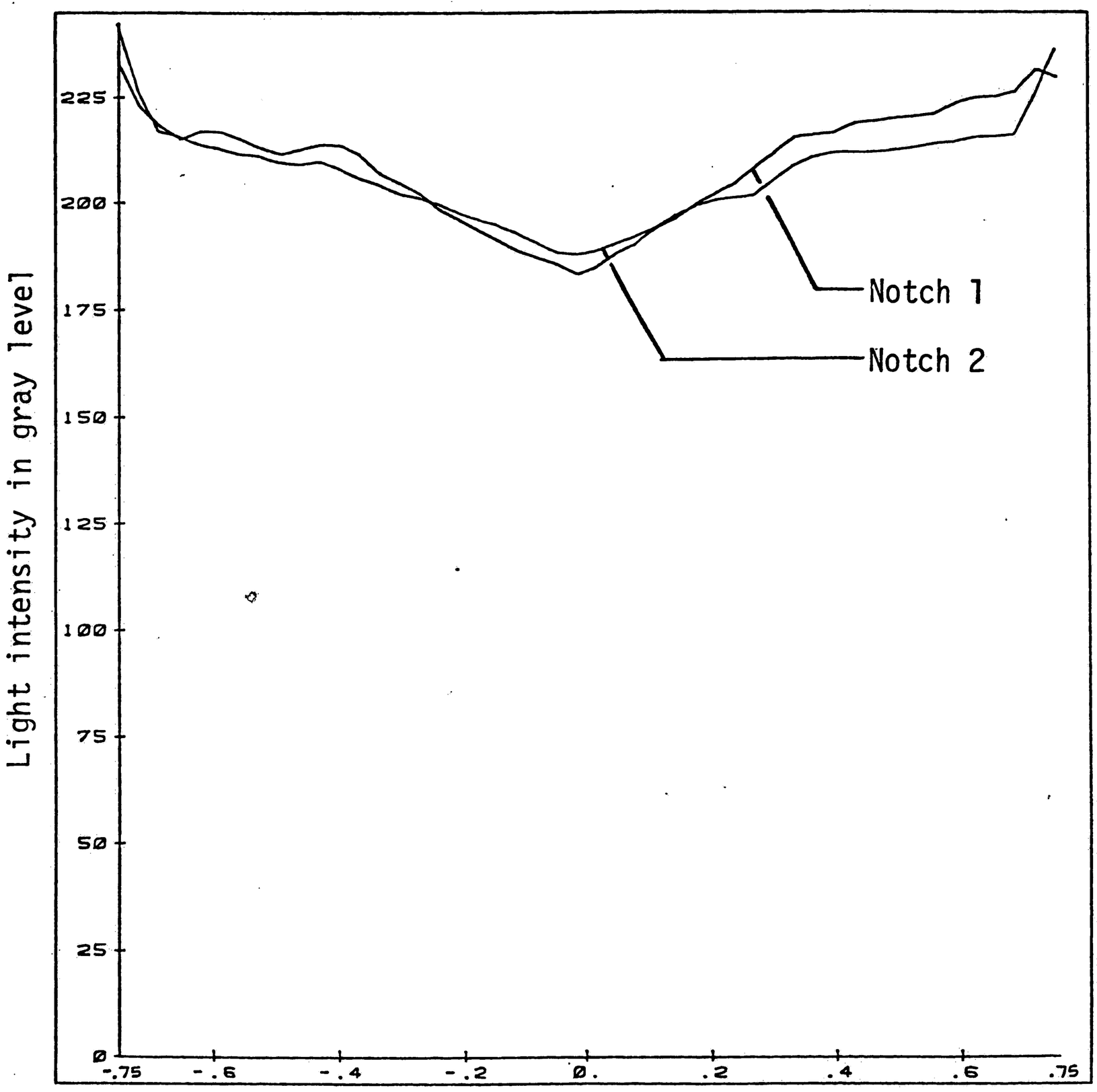

Figure 23 - Light intensity over notch region for Notches 1 and 2 at excitation C.

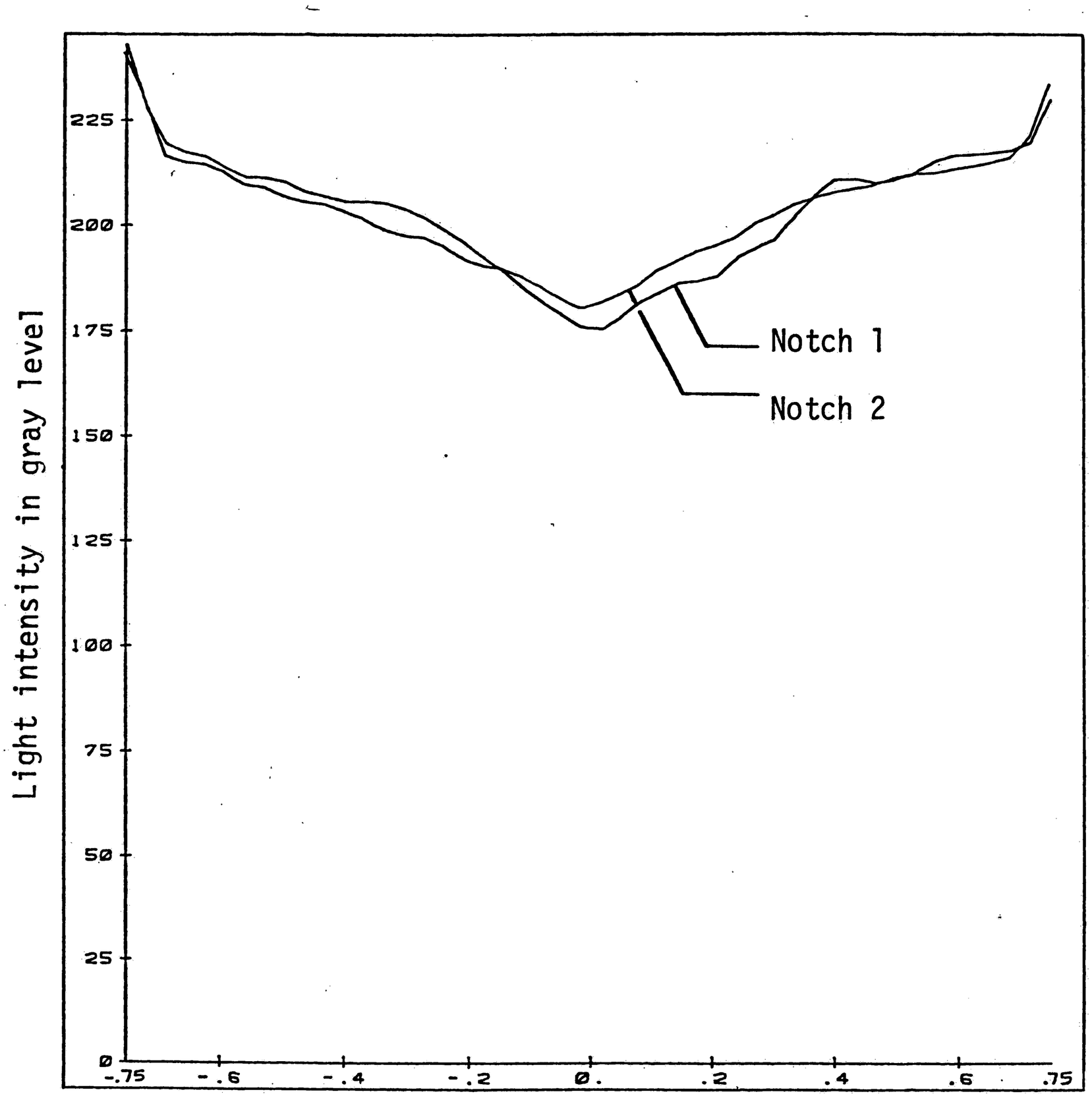

Figure 24 - Light intensity over notch region for Notches 1 and 2 at excitation D.

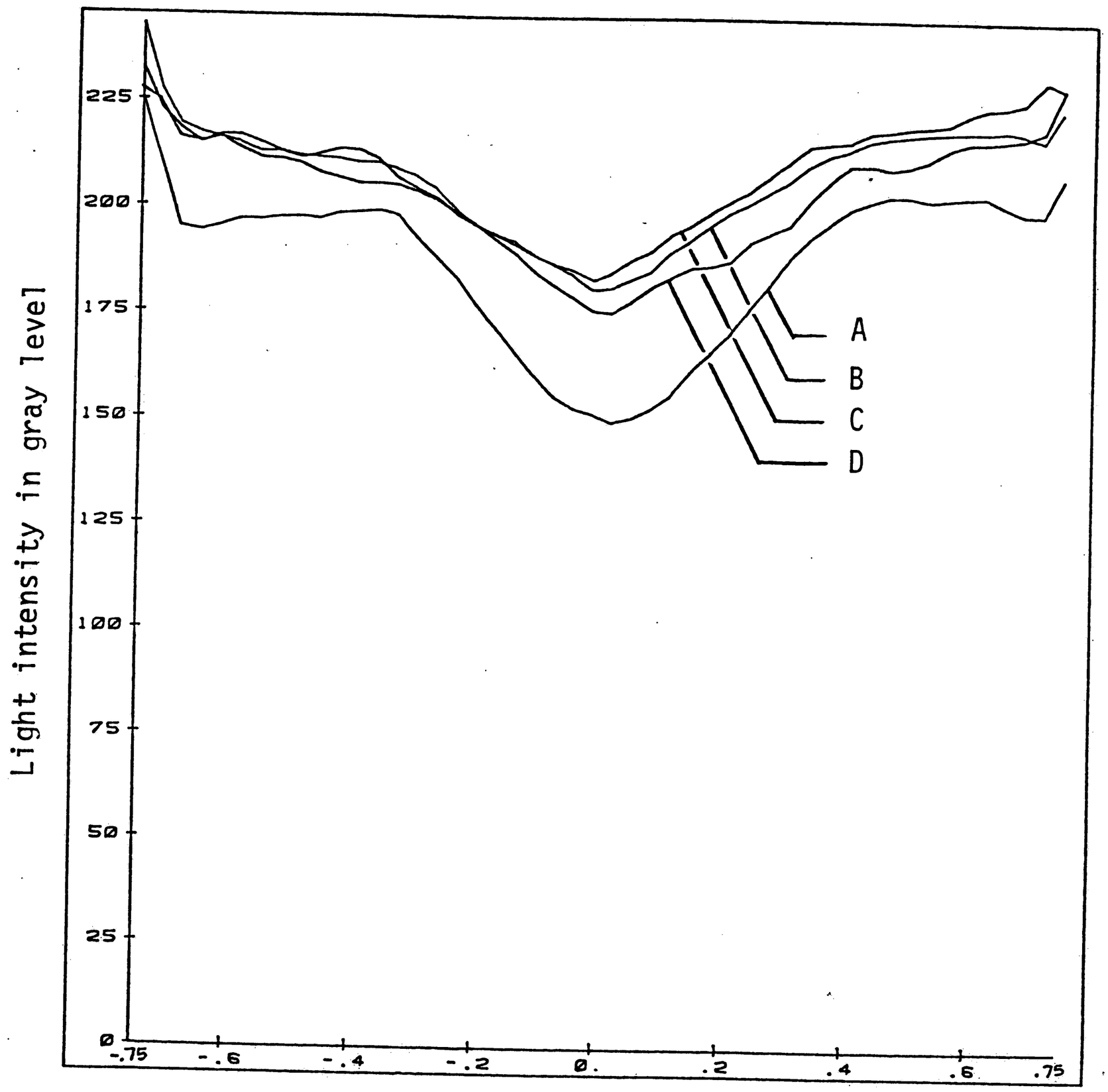

Figure 25 - Light intensity over notch region for Notch 1 at excitations A, B, C and D.

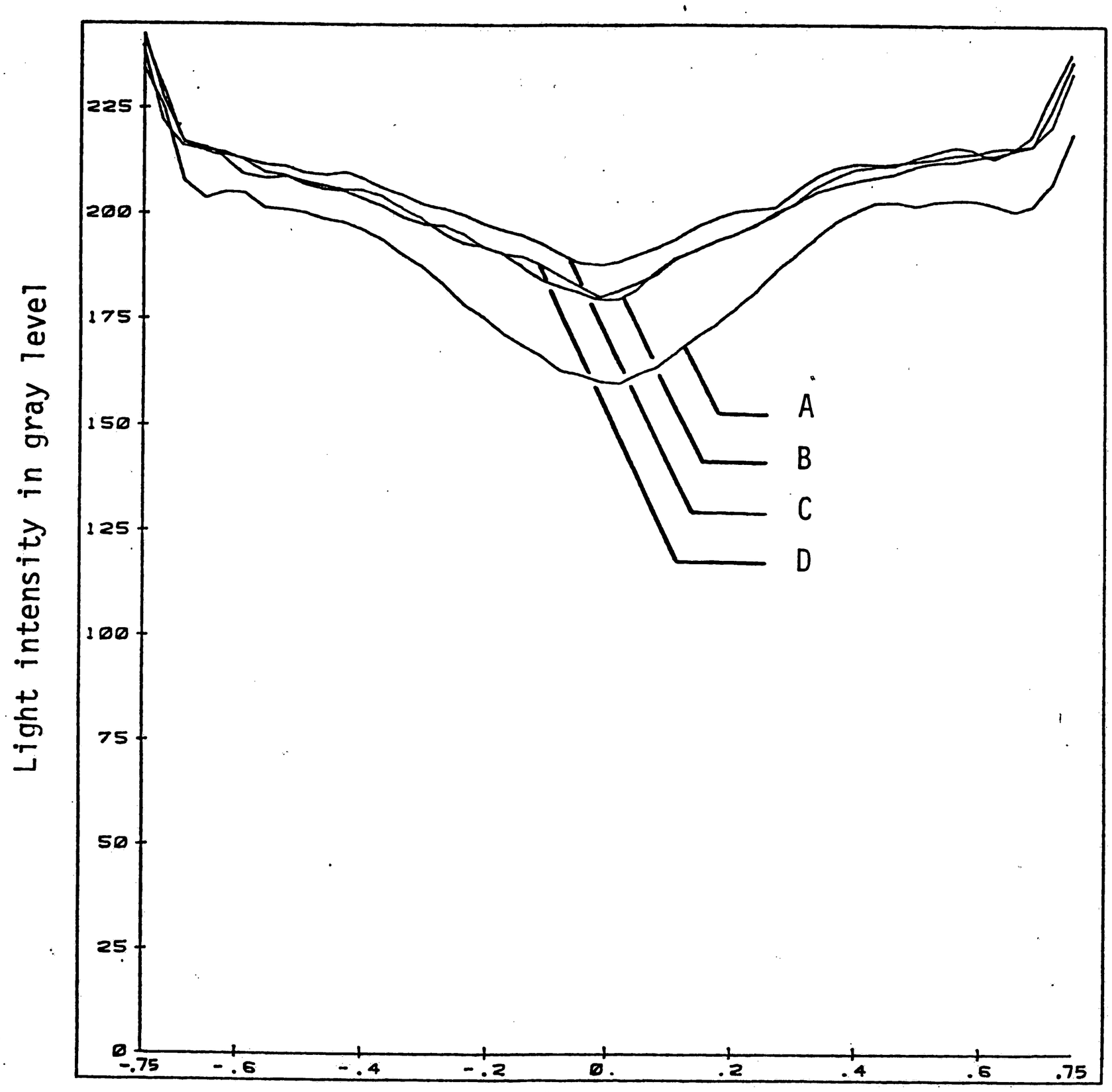

Figure 26 - Light intensity over notch region for Notch 2 and excitations A, B, C and D.

CHAPTER VI - CONCLUSIONS AND RECOMMENDATIONS FOR FUTURE RESEARCH

In contrast to the majority of the past efforts in EDI which are empirical in nature, the present investigation provided theoretical support for image pattern recognition of specimens with precut notches of different depth. The various parameters affecting EDI were studied so as to reproduce the measurements in a reliable fashion and to apply the technique for detecting mechanical imperfections in metals. Effects of the wave forms are studied by varying the excitation settings so as to obtain the best correlation between the light intensity and electric field intensity distribution. This critical attempt shows that EDI is indeed promising and can be developed to supersede all existing techniques such as Electronic Microscopy, X-ray Imaging, Thermography, Nuclear Magnetic Resonance (NMR), Mass Spectroscopy, Ultrasound Method, General Radiography as well as Photoelasticity. The same information gained by EDI in this work would require the application of several of the more conventional techniques. For example, electron microscope would be needed to detect the texture and defects on the specimen surface. Mass spectroscopy can be applied to characterize corrosive agents. Information on the three-dimensional pattern of the contaminated portion of the specimen by acid requires the use of NMR. X-ray Imaging, Radiography and Ultrasound Methods also apply.

Although some of the existing methods may yield more accurate results in some instances than EDI, they, however, are comparatively more costly as a large quantity of accessories are required. EDI technique is relatively inexpensive by orders of magnitude once the accompanying

software is developed. Needless to say, the versatility and reliability of any experimental technique depend on the soundness of the theory without which the method remains empirical. In this respect, EDI, at present, has limited support.

What is needed in the future is the development of a generalized theory that can account for the energy dissipated by thermal, mechanical and electrical effects. Their individual contribution needs to be sorted out. Promising progress has been advanced by the formulation of the energy density theory [21,22] in which all nonlinear and dissipative effects are maintained without loss in generality. This is accomplished by assuming that surface and volume energy are constantly exchanging. Such an interaction is responsible for the irreversibility of physical processes and has been neglected in the formulation of all classical theories in physics and mechanics. The experimental determination of energy dissipation based on EDI measurements is discussed in [23].

REFERENCES

[1] J. G. Michopoulos and G. C. Sih, "Electromagnetic Discharge Imaging Technique as a Means of Nondestructing Evaluation of Material Imperfections", Institute of Fracture and Solid Mechanics Technical Report IFSM-85-132, 1984.

[2] G. C. Sih and J. G. Michopoulos, "Formulation of Coupled Temperature, Moisture, Deformation and Electromagnetic Fields", Institute of Fracture and Solid Mechanics Technical Report IFSM-85-134, 1985.

[3] S. D. Kirlian, V. G. Adamenko, V. Kh. Kirlian and K. F. Shevkunov, "Technique for Inspection of the Physical State of a Metal", Inventor's Certificate No. 336586, Byull. Izobret., No. 14, 1972.

[4] L. A. Druzhkin and V. M. Timofeev, "High-Frequency Flaw Detection", in: Authors' Abstracts of Papers of Moscow Mining Institute, (in Russian), MOIP, Moscow, p. 38, 1967.

[5] D. E. Lord and R. R. Petrini, "High-Voltage Photography Applied to Materials Science", Lawrence Livermore Laboratory Technical Report, UCRL-51702, TID-4500, UC-38, 1974.

[6] D. E. Lord and R. R. Petrini, "High-Voltage Photography Applied to Nondestructive Testing", Lawrence Livermore Laboratory Technical Report, UCRL-77388, 1975.

[7] G. C. Sih and J. G. Michopoulos, "Nondestructive Detection of Damage in Aluminum: Electromagnetic Discharge Imaging", Journal of Theoretical and Applied Fracture Mechanics, Vol. 5, No. 1, pp. 23-30, 1986.

[8] A. Von Hippel, Dielectrics and Waves, Wiley, New York, 1954.

[9] J. C. Anderson, Dielectrics, Reinhold Publishing Corporation, London, 1964.

[10] V. V. Daniel, Dielectric Relaxation, Academic Press, London, 1967.

[11] S. Kirlian, Zhurnal Nauchnoi i Prikladnoi Fotograffii i Kinematograffii, 6, p. 397, 1961.

[12] S. Kirlian and V. Kirlian, "Photography by Means of High-Frequency Currents", in: Galaxies of Life, S. Kripner and D. Rubin, Gordon and Breach, 1973.

[13] S. Kripner and D. Rubin, eds., Galaxies of Life, Gordon and Breach, 1973.

[14] S. Prat and J. Schlemmer, "Electrophotography", Journal of the Biological Photographic Association, Vol. 7, No. 4, June 1939.

[15] K. R. Castleman, Digital Image Processing, Prentice-Hall, Englewood Cliffs, New Jersey, 1979.

[16] F. M. Penning, Electrical Breakdown of Gases, M. M. Meek and J. D. Craggs, ed., Wiley, New York, 1978.

[17] A. Von Engel, Electric Plasmas: Their Nature and Uses, International Publications Service, Taylor and Francis, Inc., New York, 1983.

[18] O. Richardson, Proc. Cambridge Phil. Soc., Vol. 11, p. 286, 1902.

[19] O. Richardson, Phil. Magazine, Vol. 28, p. 633, 1914.

[20] R. Fowler and L. Nordheim, Proc. Roy. Soc., A, Vol. 119, p. 173, 1928.

[21] G. C. Sih, "Mechanics and Physics of Energy Density and Rate of Change of Volume with Surface", Journal of Theoretical and Applied Fracture Mechanics, Vol. 4, No. 3, pp. 157-173, 1985.

[22] G. C. Sih, Energetics of Irreversibility, Elsevier, The Netherlands, (in preparation).

[23] J. G. Michopoulos and G. C. Sih, "Experimental Evaluation of Energy Dissipation by Electromagnetic Discharge Imaging", Institute of Fracture and Solid Mechanics Technical Report, (in preparation).

VITA

Chun-Hung Kuo was born on January 7, 1953 in Taipei, Taiwan, to En-Che Kuo and Yu-Wan Yao. He graduated from the High School of Taiwan Normal University in June 1971.

The author entered Chinese Culture College in September 1971. While an undergraduate, he worked for Fu-Chuen Plastic Company. After two years in CCC, he went to military service for two years. He returned to the same company after he was discharged from the service.

The author decided to go back to school. He entered Texas A&M University in January 1980. In the meantime, he was in the cooperative program with Cameron Iron Works in Houston, Texas. He received a Bachelor of Science Degree in Mechanical Engineering in August 1983.

The author began his graduate studies at Lehigh University in August 1983. He had a health problem during the first semester at Lehigh and then went to Texas for medical treatment. He returned to Lehigh in August 1984 and worked as a research assistant for the Institute of Fracture and Solid Mechanics.